Available online at www.sciencedirect.com
SCIENCE DIRECT®
Microporous and Mesoporous Materials 72 (2004) 1–23
MICROPOROUS AND MESOPOROUS MATERIALS
www.elsevier.com/locate/micromeso

Review

Molecular sieves as host materials for supramolecular organization

Dominik Brühwiler, Gion Calzaferri *

Department of Chemistry and Biochemistry, University of Bern, Freiestrasse 3, CH-3000 Bern 9, Switzerland

Received 21 October 2003; received in revised form 8 March 2004; accepted 12 March 2004
Available online 18 May 2004

Abstract

The use of zeolites and mesoporous silicas (M41S family) as host materials for the supramolecular organization of organic dye molecules, metal sulfide clusters, and transition metal complexes is reviewed. For dye–zeolite systems, different stages of organization are discussed, ranging from the arrangement of the dyes in the zeolite channels to the specific adsorption of molecules at the channel entrances and finally to the coupling of the dye–zeolite crystals to an external device. The synthesis of metal sulfide nanoparticles in zeolites is illustrated by our studies of silver sulfide clusters in zeolite A. Starting from an activated Ag^+-loaded zeolite, the synthesis exploits the defined structure of the zeolite framework to achieve controlled cluster growth yielding composites with unique luminescence properties. The organization of guest species in mesoporous silicas of the M41S family is mostly related to the chemistry of the surface silanol groups. This aspect is discussed with particular emphasis on the functionalization with organic chromophores and the grafting of isolated transition metal centers through oxo-bridges.

Keywords: Zeolite; Mesoporous silica; Supramolecular organization; Inclusion of organic dye molecules and semiconductor clusters; Grafting of transition metal complexes

Contents

1. Preface . . . 2

2. Supramolecular organization of organic dye molecules in zeolites . . . 2
   2.1. Introduction . . . 2
   2.2. First stage of organization . . . 3
      2.2.1. Insertion and diffusion . . . 3
      2.2.2. Determination of loading levels . . . 7
      2.2.3. Orientation . . . 7
      2.2.4. Interaction between the dye molecules . . . 9
      2.2.5. Interaction of the dye molecules with the zeolite . . . 10
   2.3. Second stage of organization . . . 11
   2.4. Third stage of organization . . . 12
      2.4.1. Macroscopic ordering . . . 12
      2.4.2. Coupling to external devices . . . 12

3. Supramolecular organization of metal sulfide particles in zeolites . . . 13
   3.1. Introduction . . . 13
   3.2. From silver ions to silver sulfide clusters . . . 14
      3.2.1. Silver ions in zeolite A . . . 14
      3.2.2. Silver sulfide cluster growth . . . 14

* Corresponding author. Fax: +41-31-6313994.
E-mail addresses: dominik.bruehwiler@iac.unibe.ch (D. Brühwiler), gion.calzaferri@iac.unibe.ch (G. Calzaferri).

1387-1811/$ - see front matter © 2004 Elsevier Inc. All rights reserved.
doi:10.1016/j.micromeso.2004.03.027

3.3. Properties of silver sulfide clusters in zeolite A . . . 15
3.3.1. Theoretical considerations . . . 15
3.3.2. Photoluminescence . . . 15

4. Supramolecular organization in materials of the M41S family . . . 16
4.1. Introduction . . . 16
4.2. Inclusion of organic dyes in M41S materials . . . 17
4.3. Isolated transition metal centers in M41S materials . . . 18
4.3.1. General concepts . . . 18
4.3.2. Framework substitution . . . 18
4.3.3. Postsynthetic modification . . . 18

5. Summary and outlook . . . 20

Acknowledgements . . . 20

References . . . 20

1. Preface

The term *Supramolecular Organization* refers to entities of higher complexity resulting from the association of two or more chemical species held together by intermolecular forces. Molecular sieves are ideal host materials for supramolecular organization, providing high chemical, mechanical, and thermal stability. The defined geometry of the cavities and channels can be transferred to the spatial arrangement of guest species, thereby generating highly structured materials. Further functionalities can be added by assembling molecular sieve crystals into well-defined macroscopic structures on various supports [1–4] and by allowing communication between guests and external species or devices [5]. The large variety of molecular sieves featuring different pore structures and morphologies offers multiple possibilities for the design of host–guest systems with specific properties. In this review we will mainly focus on results from our laboratory covering supramolecular organization of organic dye molecules and metal sulfide clusters in zeolites L and A, respectively (Sections 2 and 3). Aspects of supramolecular organization in the rapidly developing field of mesoporous molecular sieves of the M41S family will be discussed in Section 4. Readers are referred to Ref. [6] for a review on chromophores in porous silicas and minerals. The aspect of photochemistry in zeolites has recently been extensively reviewed by Hashimoto [7].

The properties of guest–zeolite composites can be influenced dramatically by impurities (transition metals, chloride) often present in commercially available zeolites. We therefore generally work with highly pure zeolite A and zeolite L, the synthesis of which is described in Refs. [2,8], respectively. In addition to the purity of a zeolite sample, the size and morphology has to be considered important as well, especially when the guest–zeolite composites are to be coupled to external devices [5] or arranged in a defined macroscopic structure. Methods for tuning the size and shape of zeolite L crystals—a prerequisite for the realization of applications based on dye–zeolite L composites—are reported in Ref. [8].

2. Supramolecular organization of organic dye molecules in zeolites

2.1. Introduction

The structural properties of zeolites, i.e., defined cages and channels of uniform sizes, are ideal for obtaining highly organized arrangements for a large variety of organic dye molecules. Our research has been focusing on zeolite L as host material. Its one-dimensional channel system allows the synthesis of highly anisotropic dye–zeolite composites. Due to their ability to efficiently collect and transport energy over relatively large distances, these composites constitute artificial photonic antenna systems. The zeolite thereby prevents the formation of undesirable dye aggregates which generally exhibit fast radiationless decay [9]. We have recently demonstrated that the size of zeolite L crystals can be tuned between 30 and 3000 nm by changing the composition of the starting gel [8]. Control of the morphology and size of the crystals allows optimization of the dye–zeolite composites for a specific application. Large crystals are useful for studying the photophysical properties of the dye–zeolite composites by means of optical microscopy methods. Crystals smaller than a few hundred nanometers, on the other hand, are needed for high efficiency photonic antennae. Small dye-loaded crystals can further be used as fluorescent probes in cell biology and analytical chemistry [10], for developing a

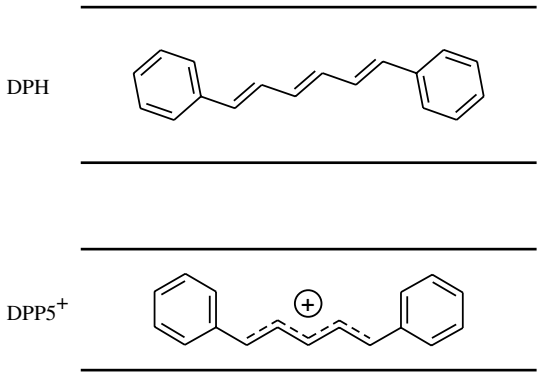

Fig. 1. Two examples of increased stability of organic guests in zeolite channels: 1,6-diphenylhexatriene DPH in zeolite L (top) [11] and 1,5-diphenylpentadienylium cation $DPP5^+$ in ZSM-5 (bottom) [13].

new generation of dye-sensitized solar cells, or for designing novel light emitting diodes [5].

An important advantage of dye–zeolite composites is the protection of the dye molecules against chemical attack, photobleaching or thermal decomposition. The light sensitive 1,6-diphenylhexatriene (DPH) for example is considerably stabilized when inserted into zeolite L, because the available space for *trans* to *cis* isomerization is insufficient (see Fig. 1) [11]. Protection from chemical attack is observed in many cases where reactive molecules have to overcome a large diffusional barrier or where anions such as hypochlorite cannot enter the negatively charged channels [8,12]. García and coworkers [13] observed that inclusion of α,ω-diphenylallyl cations (DPP) into ZSM-5 leads to a major increase in their stability against reaction with H_2O. It was suggested that the phenyl caps of the included DPPs are acting as molecular stoppers, protecting the positive DPP centers from attack by external nucleophilic reagents (see Fig. 1).

The substantially increased stability of organic dye molecules in zeolites opens possibilities for producing new kinds of pigments. High brightness can be created by inclusion of fluorescent molecules and a large variety of colors becomes accessible through combination of two or more dyes. Tables 1 and 2 show the dye molecules we have incorporated into zeolite L. Cationic molecules (Table 1) are loaded by ion exchange from solution, while neutral molecules (Table 2) are adsorbed from the gas phase or from a solution with solvent molecules too large to enter the zeolite channels. Inclusion of an anionic dye was accomplished by adsorption of the neutral dye resorufin (ResH) from the gas phase and subsequent deprotonation through exchange of the hydroxyl protons with potassium ions [14]. A new and convenient strategy for synthesizing pure oxonine (Ox^+), a molecule we have used in a variety of studies involving dye–zeolite composites [8,15–17], was reported recently [18]. The laser emission which was observed for Ox^+-loaded zeolite L crystals [19] is currently being investigated. The inclusion of naphthalene and anthracene into zeolite L was studied by Hashimoto et al. [20]. Pyrene–zeolite L composites were investigated by Liu and Thomas [21].

The following discussion of dye–zeolite systems is divided into three sections, each describing a different stage of organization (see Fig. 2). The first stage addresses the organization of the dyes inside the channels and focuses on the dye molecules themselves. Aspects of insertion and diffusion, orientation inside the channels, and interaction with the environment (other dye molecules, zeolite framework and cations) will be covered in separate subsections. The second stage of organization deals with so-called stopcock molecules. These molecules which are specifically positioned at the very end of the channels are used to trap electronic excitation energy from donor molecules inside the crystal or inject electronic excitation energy to acceptor molecules in the channels. They also provide additional stability by preventing the included molecules from leaving the channels or by excluding reactive molecules. Finally, the third stage of organization describes the coupling of the dye–zeolite composites to an external device and the arrangement of the crystals into ordered macroscopic structures.

2.2. First stage of organization

2.2.1. Insertion and diffusion

The two most frequently used methods for the incorporation of dye molecules into the cavities of zeolites are adsorption from the gas phase [11,20] and ion exchange from solution [22]. In the latter case, the ion exchange equilibrium can be influenced in favor of the dye-loaded zeolite by using an ionophore crypt to trap the exchanged alkali ions [18,23]. For a detailed review of different inclusion methods see Ref. [24]. Irrespective of the inclusion method, care has to be taken to assure that the outer surface of the zeolite crystals is free of dye molecules, which is generally well accomplished by repeated washing with a suitable solvent. Cationic dyes have the tendency to form aggregates on the outer surface, featuring photophysical properties distinctively different from the corresponding monomers in the channels [12,25]. A similar observation has been made for the adsorption of anthracene on NaY, where molecules at the outer surface are identified by their excimer emission [7]. Furthermore, solvatochromy can be used for checking whether dye molecules are located on the outer surface. In this method, the dye-loaded zeolite crystals are suspended in a solvent which for reasons of polarity or sterical hindrance cannot enter the zeolite channels. Molecules on the outer surface will then experience a different environment and their electronic

Table 1
Cationic dyes and radicals incorporated into zeolite L

Name/abbreviation	Structural formula	Name/abbreviation	Structural formula
Proflavin$^+$	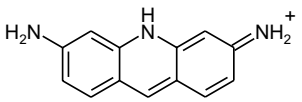	MV^{2+}	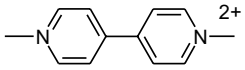
Py^+	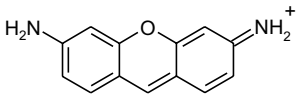	BDP^+	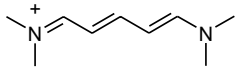
$PyGY^+$	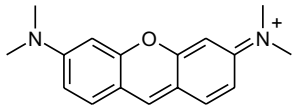	MC^+	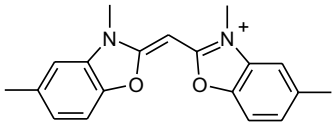
PyB^+	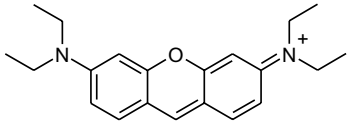	$BTMPI^+$	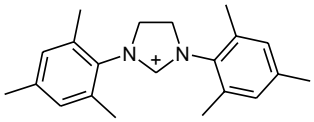
Ox^+	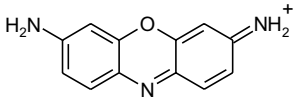	DSM^+ ($n = 1$)	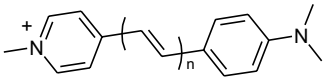
$DEOx^+$	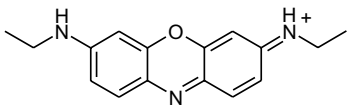	Hydroxy-TEMPO	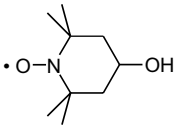
Th^+	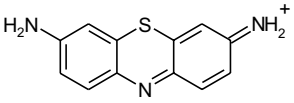		

absorption spectrum will exhibit a shift depending on the solvent [12,25].

Extending the information obtained from classical methods [26], the kinetics of insertion and intrachannel diffusion of dye molecules in zeolite L was studied by using the pronounced distance dependence of the electronic excitation energy transfer between pyronine (Py^+) and oxonine (Ox^+). The two molecules were found to have very similar diffusion coefficients (1.0×10^{-20} $m^2\,s^{-1}$ at 54 °C) [17]. Few intrachannel diffusion studies have so far been carried out on molecules as large as Py^+ or Ox^+. Hashimoto et al. [27] reported diffusion coefficients for azulene, ferrocene, and anthracene in NaY based on triplet quenching experiments. Values were ranging from 10^{-15} to 10^{-16} $m^2\,s^{-1}$ at ambient temperature, which is still considerably slower than the values observed for benzene [28], thereby clearly illustrating the size dependence of the diffusivity. However, it has to be noted that the diffusivity not only depends on the molecular size but also on specific interactions with the zeolite. A diffusion coefficient as small as 10^{-18} to 10^{-19} $m^2\,s^{-1}$ was obtained for benzene in CaY indicating a stronger host–guest interaction compared to the benzene–NaY system [29].

The mobility of guest molecules in zeolites often depends on the level of hydration. Measurement of the triplet decay constants of anthracene in NaY revealed that the adsorption of water first leads to a considerable increase of the decay constant [30]. This effect was attributed to the cancellation of adsorption interactions between the anthracene molecules and the zeolite walls, due to the much stronger affinity of the zeolite towards the co-adsorbed water molecules. Ultimately, the higher mobility of the anthracene molecules allows self-quenching and triplet–triplet annihilation. However, further increasing the amount of adsorbed water was followed by a decrease of the triplet decay constants, therefore indicating a decrease of mobility

Table 2
Neutral dyes incorporated into zeolite L

Name/abbreviation	Structural formula	Name/abbreviation	Structural formula
BP	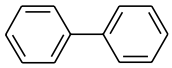	DXP ($n = 0$) DXT ($n = 1$)	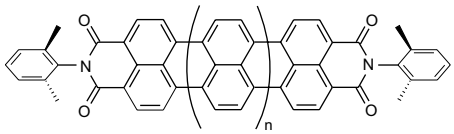
*p*TP	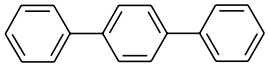	Isoviolanthrone	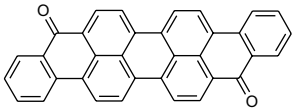
DPH	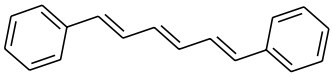	ResH	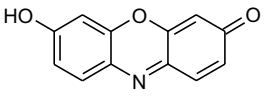
N-ethylcarbazole	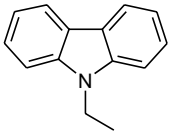	PBOX	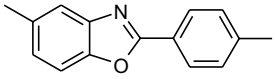
Fluorenone	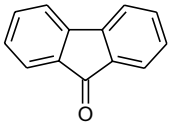	MBOXE	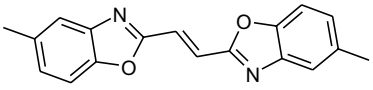
DCS	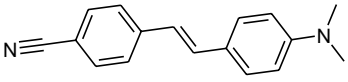	POPOP	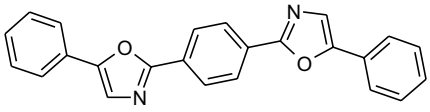
Stilbene	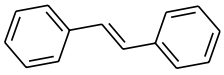	DMPOPOP	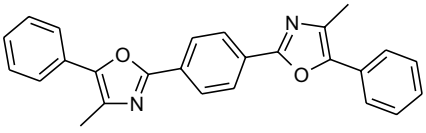
Naphthalene[a]	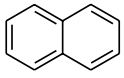	Azobenzene	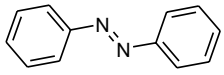
Anthracene[a]	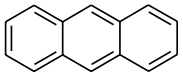	Pyrene[b]	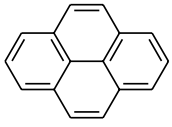

[a] Ref. [20].
[b] Ref. [21].

caused by increased blocking of the windows connecting the cages and reduction of the free volume inside the cages by water molecules [30]. As we will see in Section 3, the effect of adsorbed water molecules on the mobility of guest species is of special importance for the process of silver sulfide cluster formation in zeolite A [31,32].

Adsorption of water can in some cases lead to the liberation of guest molecules. This effect was studied in detail for resorufin (ResH) in zeolite L [14]. After insertion from the gas phase, the incorporated ResH molecules were deprotonated to yield Res^-. While this anionic dye is strongly fluorescent in solution, complete quenching occurs when it is located in the channels of

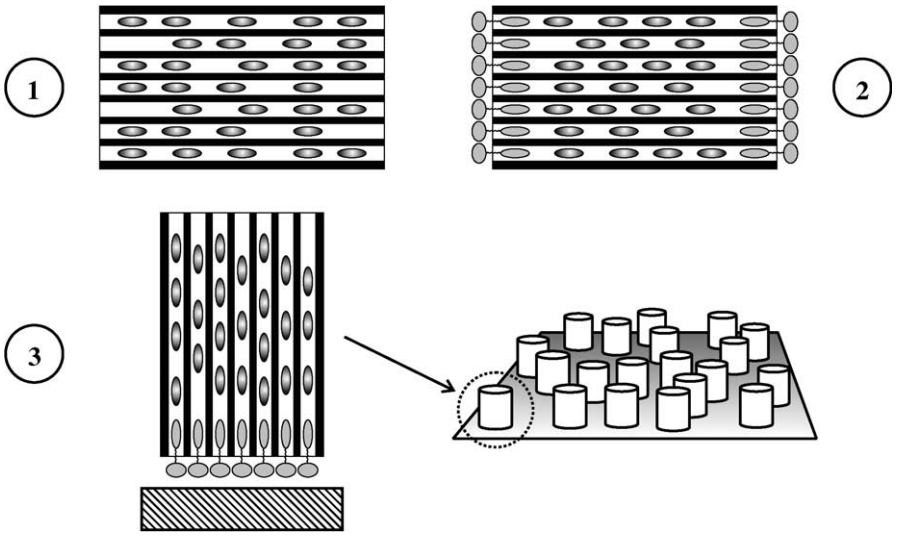

Fig. 2. Schematic illustration of the three stages of organization.

potassium zeolite L. We utilized this effect to investigate the liberation of the incorporated Res^- molecules in function of various co-adsorbed solvents. The liberation of Res^- from the zeolite into the surrounding solution constitutes an irreversible process, since, due to its anionic nature, Res^- cannot reenter the zeolite channels. Measurement of the fluorescence intensity of a suspension of Res^--loaded zeolite therefore directly indicates the ability of the respective solvent to mobilize the incorporated Res^- molecules. The following series for the amount of liberated Res^- was found:

$$\text{water} \gg \text{methanol} > \text{ethanol} > \text{1-propanol} \gtrsim \text{1-butanol}$$

No liberation of Res^- was observed upon suspending the loaded zeolite in 1-butanol despite a similar solubility of the dye compared to the other solvents. The above series clearly indicates that with increasing size of the solvent molecules, mobilization of Res^- inside the channels becomes less efficient. This effect is not attributed to sterical hindrance upon entering the channels (all of the above solvents are small enough to easily fit into the channels of zeolite L), but rather to constraints upon passing the incorporated Res^- molecules [14]. This finding has proven to be valuable for the removal of dye molecules on the outer surface without liberating those in the channels. Provided that the respective dye is soluble in 1-butanol, repeated washing of the dye–zeolite composite with this solvent usually results in a clean outer surface, while the dye molecules in the channels remain unaffected.

Reversibility of the displacement by water was observed for *p*-terphenyl (*p*TP) in zeolite L [11]. Fig. 3 shows the amount of intrazeolite *p*TP in function of the hydration state of the zeolite. Up to about 10 H_2O molecules per unit cell, almost all *p*TP remains inside the

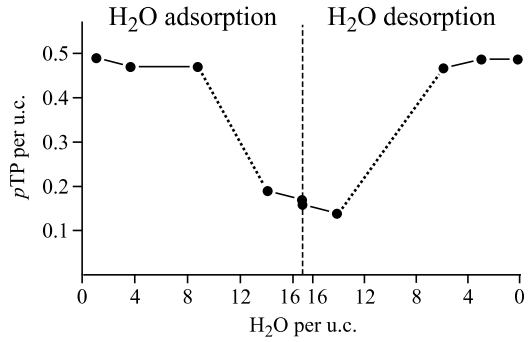

Fig. 3. Amount of included *p*TP per unit cell of zeolite L for different amounts of co-adsorbed H_2O. The H_2O content was varied by letting a dry *p*TP-zeolite sample adsorb water (left side) or by dehydration of a wet sample (right side) [11].

channels. Further increasing the water content leads to displacement of *p*TP which ultimately moves to the outer surface of the crystals. Desorption of water causes reinsertion of the *p*TP molecules. The displacement of guest molecules by water is critical for species featuring a weak interaction with the zeolite. For zeolite L, displacement can be efficiently inhibited by closing the channel entrances with suitable molecules, so-called stopcock molecules, which will be discussed in Section 2.3.

An important parameter in guest–zeolite systems is the distribution of the guest molecules inside the zeolite channels. After a series of experimental studies on this subject [11,12,24,33,34], we have developed simulation methods based on Monte Carlo algorithms to further our understanding of the distribution of dye molecules in zeolite L. As a very useful result of these simulations, we found that the distribution of the dyes among the channels and the distribution of empty sites between the

dyes in a channel can be described by explicit mathematical relationships [16].

2.2.2. Determination of loading levels

There are several methods for the quantitative determination of the loading level of a given dye–zeolite sample. An estimate usually follows from the loading procedure, where a calculated dye/zeolite ratio is used. The loading level is determined after the inclusion by subtracting the amount of dye not included, e.g., by measuring the UV–Vis absorption spectra of the exchange and washing solutions. In a more direct approach, HF solution is applied to the dye–zeolite sample to decompose the zeolite framework. After neutralization with NaOH solution and filtration, the amount of dye is calculated from the UV–Vis absorption spectrum of the supernatant [8]. The stability of the respective dye in HF solution has to be tested beforehand. An alternative fast and, most importantly, non-destructive method is provided by the evaluation of vibrational spectra. For thin zeolite layers coated on ZnSe wafers, quantitative information was obtained by using the characteristic ν_{as}(T–O–T) band as an internal standard [35,36]. In the case of methyl viologen (MV^{2+}) in zeolite L, Raman spectra turned out to be more sensitive in this respect, the narrow and well-isolated 500 cm^{-1} framework vibration being of similar intensity as the MV^{2+} bands [35].

2.2.3. Orientation

Fig. 4 illustrates three possible orientations of a dye molecule inside the zeolite L channels. Due to geometrical constraints, molecules longer than two unit cells are forced to align parallel to the channel (case **1**, e.g., POPOP, DMPOPOP, MBOXE, *p*TP, DPH, DCS). Shorter molecules tend to arrange as shown for case **2** or even **3**. A typical example for case **2** is MV^{2+} for which Rietveld refinement of X-ray data and molecular modeling revealed an angle of 27° between the main axis of the molecule and the *c*-axis of the zeolite [35]. For the dye molecules under investigation, the electronic transition dipole moment of the first $\pi^* \leftarrow \pi$ transition usually coincides with the long axis of the molecule. The orientation of the electronic transition moments with respect to the zeolite channels can be determined directly from the fluorescence polarization [37].

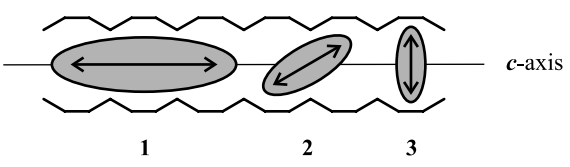

Fig. 4. Schematic illustration of different orientations of dye molecules in the main channel of zeolite L. The double arrows indicate the electronic transition dipole moment of the first $\pi^* \leftarrow \pi$ transition.

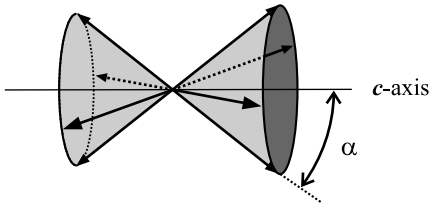

Fig. 5. Distribution of electronic transition moments of dye molecules in zeolite L described by a double cone with a half opening angle α.

A double cone distribution of the electronic transition moments as presented in Fig. 5 serves as a valuable model for interpreting fluorescence polarization measurements of the dye–zeolite composites. The distribution is characterized by the half cone angle α, which is 0° in the case where the electronic transition moments coincide with the *c*-axis of the zeolite crystal, as observed for large dye molecules (Fig. 4, case **1**). Such a crystal appears dark under a fluorescence microscope with the polarizer set perpendicular to the *c*-axis, while maximum fluorescence is observed with the polarizer set parallel to the *c*-axis. In contrary, maximum fluorescence is observed perpendicular to the *c*-axis and minimum fluorescence parallel to it if α equals 90°. This fluorescence anisotropy becomes less distinct for values of α between 0° and 90° and disappears at the magic angle of 54.7° [37].

Fig. 6 illustrates how common fluorescence microscopy readily yields information on the orientation of the electronic transition moments of molecules in the channels. Fluorescence pictures of six dye–zeolite samples are shown with different polarization of the observed single crystal fluorescence. Pictures on the left correspond to the total fluorescence, while the remaining pictures display the fluorescence with the transmitted polarization direction indicated by arrows. Note that some crystals exhibit intense fluorescence at the channel ends whereas the center remains dark. This is observed in cases where the intrazeolite diffusion of the dyes has not reached its equilibrium, thereby illustrating how the molecules enter the crystals through the openings on each side of the one-dimensional channels. For Py^+ (**A**), a relatively small molecule, maximum fluorescence is observed perpendicular to the *c*-axis, minimum fluorescence parallel to it. This indicates a rather large half cone angle α. Quantitative measurements on Ox^+ in zeolite L, which is very similar in shape and size to Py^+, revealed a half cone angle of 72° [37]. $DeOx^+$ (**B**) shows comparable behavior although being slightly larger. For $PyGY^+$ (**C**) the fluorescence anisotropy is less distinct, suggesting an angle close to 55°. Pronounced fluorescence anisotropy is observed for the ethyl-substituted PyB^+ (**D**) with maximum fluorescence detected parallel to the *c*-axis. A very similar behavior is found for DCS (**E**) and other large molecules such as POPOP (**F**), DMPOPOP or DXP, clearly indicating a half cone angle

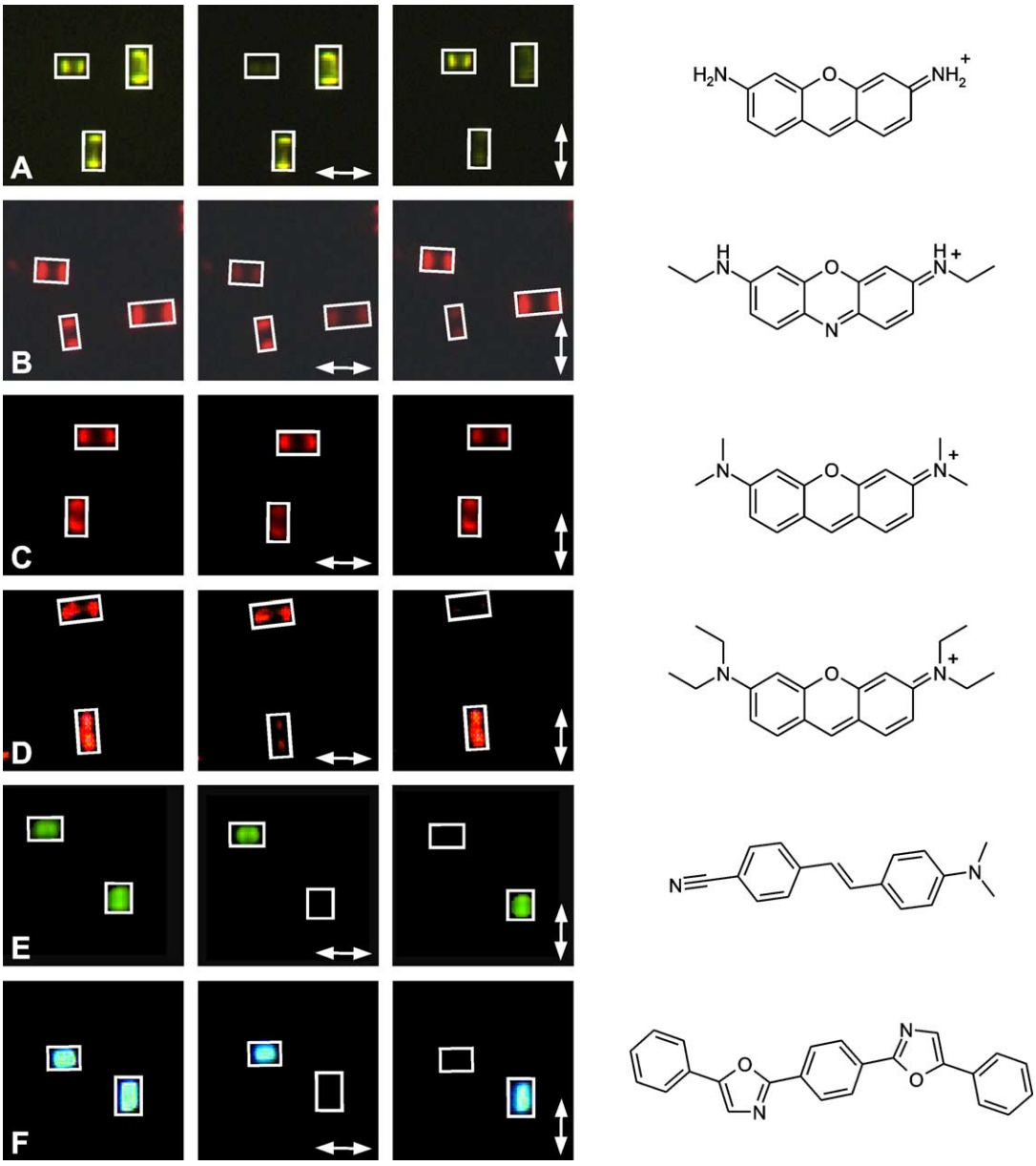

Fig. 6. Fluorescence microscopy images of dye-loaded single crystals of zeolite L without polarizer (left column) and with polarizer (center and right column). The arrows give the direction of the transmitted polarization. The length of the crystals (measured along the *c*-axis) is in the range of 1.5–2 μm. The rectangles indicate the position of the single crystals.

close or equal to 0° and thus an orientation as shown in Fig. 4, case **1**.

An interesting aspect concerning the orientation of guest species in zeolites is the light-induced reorganization, for example by photoisomerization. Azobenzene features a very distinct behavior in this respect. Hoffmann et al. [38] were able to switch between the azobenzene isomers in $AlPO_4$-5 and ZSM-5 with UV light (generating the *cis* isomer) or blue light (regenerating the *trans* isomer), thereby leading to significant changes of the optical properties of the composite. We recently observed reversible light-induced changes of the optical properties for zeolite L containing the dye MBOXE. Irradiation of the sample with monochromatic UV light (290 nm) at −190 °C leads to the development of a new luminescence band at 525 nm. Consecutive spectra taken at different times during exposure to 290 nm light show an isosbestic point at 480 nm (see Fig. 7). Heating the sample to room temperature reverses the changes. The reason for this effect is at this point not entirely clear. Conversion to the *cis* isomer is unlikely for sterical reasons. Rotation of one of the benzoxazole rings around a single-bond axis, however, has to be considered a possibility.

Due to the steric constraints imposed by the zeolite structure, many flexible molecules adopt a 'frozen'

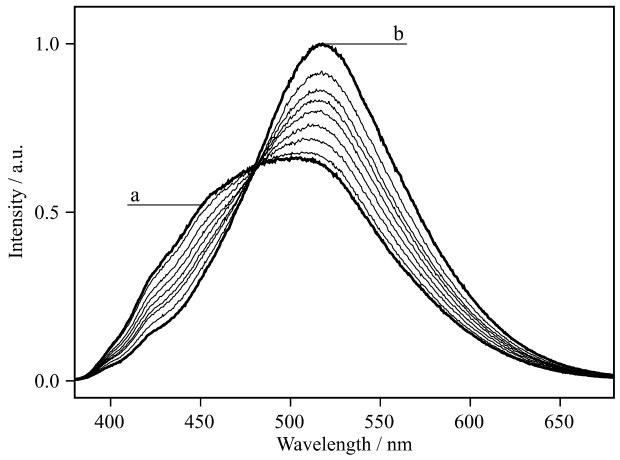

Fig. 7. Photoluminescence spectra of MBOXE in zeolite L at different times during exposure to 290 nm light at a constant temperature of −190 °C: Before exposure (spectrum a) and after a total exposure time of 30 min (spectrum b). The spectra were measured at −190 °C by excitation at 350 nm.

conformation inside the channels, which can cause significant changes of their photophysical properties. Scaiano and coworkers [39] observed such an effect in the case of β-phenylpropiophenones (β-PP) in silicalite. While β-PP does not phosphoresce in solution, strong phosphorescence was found for the β-PP-silicalite composites. It was concluded that the folded molecular conformation responsible for the efficient intramolecular quenching of the excited carbonyl triplet cannot be adopted when the molecules are inside the silicalite channels (see Fig. 8).

2.2.4. Interaction between the dye molecules

In our research on artificial photonic antenna systems, we have been mainly interested in dye–zeolite L composites consisting of a high concentration of monomeric dye molecules. An arrangement as shown in Fig. 9 (top) features no orbital interaction between the dye molecules and is ideal for transporting electronic excitation energy in analogy to the mechanism used in the antenna system of the photosynthetic unit of green plants. Molecules occupying more than two unit cells of zeolite L generally adopt such an arrangement. Negligible electronic coupling was also achieved with smaller dyes (e.g., Ox^+ or Py^+) featuring large α values. More flexible molecules have the option to arrange as shown in the lower part of Fig. 9, where partial overlap causes alteration of the optical properties of the dye–zeolite composite. Specific substituents shielding both ends of the molecule, as for example in DXP, help to avoid such situations.

An arrangement as shown in the upper part of Fig. 9 prevents the dye molecules from gliding past each other. The spatial confinement therefore allows the filling of specific parts of the channels with a desired type of dye. This is the basis for the preparation of a system capable of efficiently transporting electronic excitation energy. The transport is possible due to a near field interaction between an electronically excited molecule and a molecule in the ground state. The dominant term is usually a dipole–dipole interaction term and hence is proportional to R^{-6}, where R is the center-to-center distance between the two interacting molecules. The critical interaction distance R_0 (distance at which the energy transfer is 50% efficient) is in the order of a few nanometers for organic chromophores. R_0 is also called "Förster radius", after Theodor Förster who was the first to understand this excitation energy transfer process from a molecule in the excited state to an acceptor molecule in the ground state [40]. Fig. 10 (top) illustrates the functionality of a dye–zeolite L photonic antenna. Light is first absorbed by one of the strongly luminescent dye molecules in the channels. Due to the short distances and the ordering of the electronic transition dipole moments, the electronic excitation energy can be transported by Förster energy migration to a specific trap (acceptor) at the channel ends. Transport of the excitation energy thereby occurs preferentially along the c-axis. Theoretical considerations of energy migration as a series of Förster energy transfer steps indicate that energy migration rate constants of up to 30 steps/ps can be expected in such materials [41]. For a detailed theoretical account of Förster energy transfer in dye-loaded zeolite L see also Ref. [33].

A typical bidirectional photonic antenna is prepared by first inserting Py^+ (= donors) followed by insertion

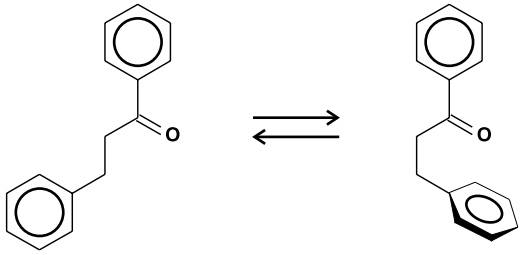

Fig. 8. Rotation leading to a folded conformation of β-PP, thereby allowing efficient intramolecular quenching of the phosphorescence [39].

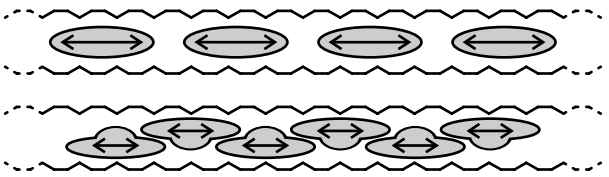

Fig. 9. Orientation of large molecules in the main channel of zeolite L. The molecules and the electronic transition dipole moments of the first $\pi^* \leftarrow \pi$ transition are aligned parallel to the channel axis (c-axis) without (top) or with (bottom) electronic interaction.

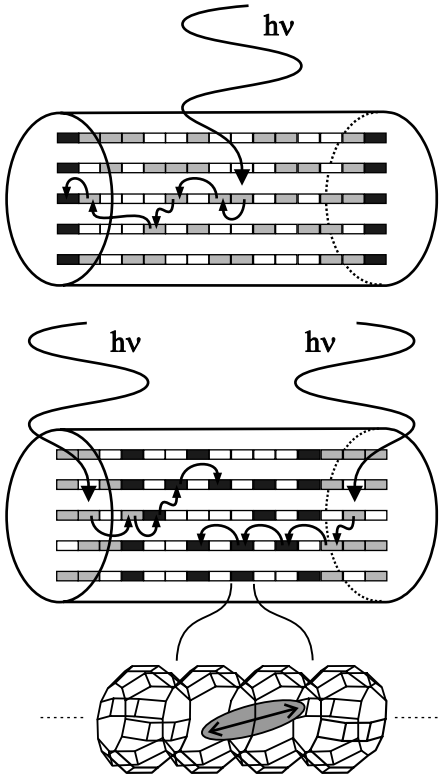

Fig. 10. Schematic illustration of a cylindrical zeolite L crystal consisting of organized dye molecules acting as donors (light grey rectangles) and acceptors (dark grey rectangles). Top: The donors are located in the middle part of the crystal, the acceptors at the front and back of each channel. Electronic excitation energy is thus transported from the center to the channel ends. The functionality of the inverse system is illustrated below. The enlargement shows details of a channel with a dye and its electronic transition moment (arrow).

of Ox^+ (= acceptors) [42]. The efficiency at which electronic excitation energy is transferred by a Förster mechanism to the acceptors at both ends of the channels depends on the mean distance between the donors among which the energy migrates. The transfer efficiency is further determined by the length of the zeolite crystals [8]. Longer crystals require more migration steps and therefore increase the probability that the excitation energy dissipates by spontaneous emission or thermal relaxation. Time-resolved luminescence measurements support the interpretation of excitation energy transport by a Förster mechanism: For crystals containing either Py^+ or Ox^+, a single exponential luminescence decay is observed under oxygen-free conditions. The main characteristic of the luminescence decay of crystals containing both dyes in an arrangement as shown in Fig. 10 is that the acceptor (Ox^+) intensity first increases before it starts to decay. This initial intensity increase becomes faster with increasing donor (Py^+) loading [16]. We have recently extended the photonic antenna concept to systems containing three different dyes, thereby covering a wide absorption range in the visible and near UV [11,34]. Placing the acceptor molecules in the middle part of the zeolite channels and the donor molecules at the ends reverses the function of the photonic antenna (see Fig. 10). Electronic excitation energy can now be transported from the ends of the channels to the centers. While such a system constitutes an additional tool for exploring the energy migration mechanism, it is also of practical importance, i.e., for developing a new generation of LEDs [24].

The systems described above constitute bidirectional antennae. Due to the symmetric arrangement of different dye molecules (sandwich structures [11]) excitation energy is transported through the one-dimensional channels in both directions. The synthesis of monodirectional (asymmetric) antennae, where this transport occurs in one direction only, is currently under investigation in our laboratory.

2.2.5. Interaction of the dye molecules with the zeolite

Sites of preferred adsorption in the cavities or channels of a zeolite are usually associated with extra-framework cations and framework oxygens. Interaction with extra-framework cations can have a significant effect on the photophysical properties of the guest molecules. Ramamurthy et al. [43] observed that the presence of heavy atoms considerably increases the phosphorescence intensity of incorporated aromatic species such as naphthalene. Exchanging some of the extra-framework cations with protons affects the pH inside the main channel of zeolite L. The intrazeolite pH was probed by inserting dye molecules which exhibit a change in the electronic absorption spectrum upon protonation (e.g., Th^+ and DSM^+) [24]. Similarly, different extra-framework cations lead to different intrazeolite pH values. This effect was attributed to the different pK_a values of the respective hydrated ions [44]. The intrazeolite pH values of different cation-exchanged samples of zeolite L ultimately showed the same trend as observed for the corresponding cations in solution [24]:

$$pH(Mg^{2+}) < pH(Ca^{2+}) < pH(Li^+) \approx pH(K^+)$$

The most important interaction between zeolites and aromatic molecules is the well-known cation–π interaction [45]. Kaanumalle et al. [46] observed that the *cis* to *trans* isomerization of 1,2-diphenylcyclopropane does not occur when the molecule is included into zeolite Y. The stability of the *cis* isomer was attributed to an interaction between a cation and the two phenyl rings resulting in a sandwich-type arrangement. Kirschhock and Fuess [47] studied the orientation of *m*-dinitrobenzene in NaY by powder diffraction methods and concluded that polar interactions with the cations significantly affect the positioning of the guest molecules. The cations thereby have to be considered mobile as well, assuming positions where coordination to oxy-

gen either belonging to the framework, residual water, or guest molecules is possible. *m*-Dinitrobenzene was found to be located in a way to ensure interaction of the highly polar nitro groups with as many cations as possible. Preferential arrangements furthermore generally feature minimum steric hindrances between guest and framework.

2.3. Second stage of organization

Extension beyond the interior of the zeolite crystals is the quintessence of the second stage of organization and is achieved by selectively positioning molecules at the entrances of the zeolite channels. The properties of these so-called stopcock molecules are designed to allow communication between the guest molecules on the inside with materials or molecules on the outside. Furthermore, they can prevent small molecules like H_2O (often leading to liberation of guests, see Section 2.2.1) or O_2 from diffusing into the interior of the crystals. Typical stopcock molecules are composed of three parts: A narrow label which can penetrate into the channels of the zeolite, a head too large to enter the channels, and a flexible spacer connecting head and label. We distinguish between reversible stopcocks [48,49] attached to the channel entrances by adsorption and irreversible ones anchored by covalent bonds. An example for each type is shown in Fig. 11. Both molecules are coumarin derivatives with the coumarin moiety featuring as the label.

In order to adsorb a reversible stopcock molecule, its interaction with the zeolite surface needs to be stronger than its interaction with the solvent. Using a solvent in which the stopcock molecules are close to insoluble (i.e., non-polar solvents for polar stopcock molecules) not only answers this problem, but furthermore avoids the formation of aggregates by requiring very low concentrations [48]. Labels with polar moieties, especially carbonyl groups, have proven to be advantageous due to their specific interaction with sites inside the channels.

An irreversible stopcock has to provide a moiety able to undergo a reaction with surface hydroxyl groups of the zeolite to yield at least one covalent bond. Alkoxysilane groups are widely used for the modification of silica surfaces. 3-Aminopropyltriethoxysilane for example is a common reactant for this purpose [50]. Reaction in dry solvent, usually toluene, leads in this case to nucleophilic displacement of the silane ethoxyls by surface hydroxyls, resulting in the liberation of ethanol and the formation of Si–O–Si linkages. An irreversible stopcock molecule as shown in the lower right part of Fig. 11 is first adsorbed by incorporation of the label and subsequently covalently anchored by reaction of the ethoxysilane groups with surface hydroxyl groups located at the channel entrances.

Since we are mainly interested in communication via energy transfer, the stopcock molecules need to contain a strongly fluorescent unit. Depending on the application, the fluorophore can be located on the head [48] or on the label moiety [49]. In the latter case the

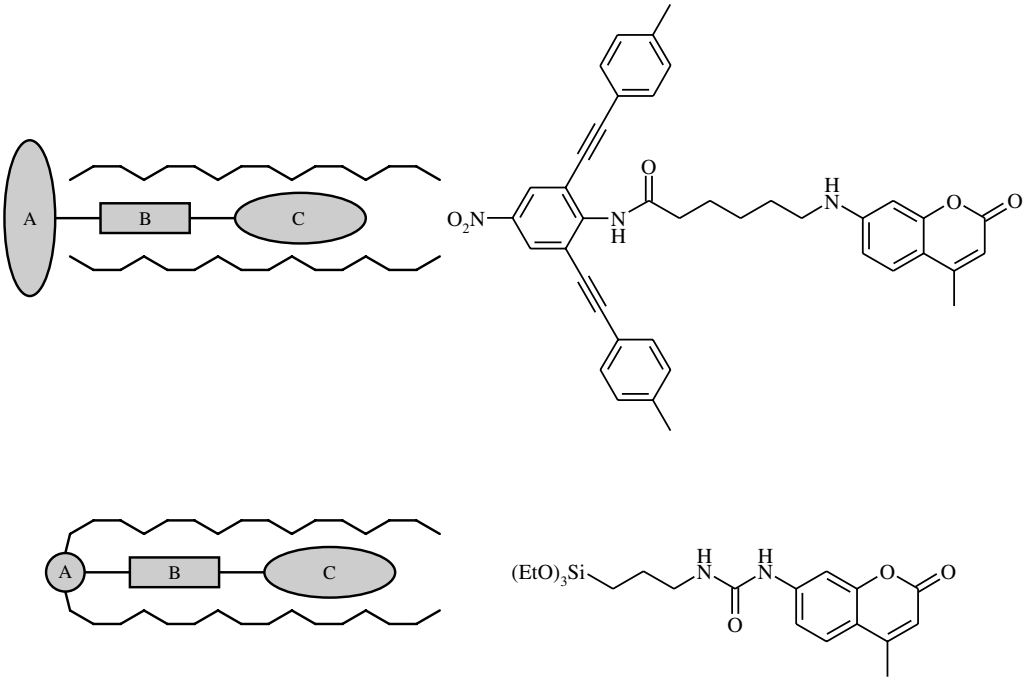

Fig. 11. Schematic illustration of reversible (top) and irreversible (bottom) stopcock molecules consisting of head (A), spacer (B), and label (C). Examples are shown on the right.

fluorophore is protected by the zeolite framework and the formation of dimers is restricted. Fluorescent head moieties on the other hand have the advantage of being closer to the external surface, which is desirable for communication with the environment. Efficient trapping or injection of excitation energy furthermore requires a sufficiently large spectral overlap between the stopcock molecules and the donor or acceptor molecules inside the zeolite channels.

2.4. Third stage of organization

2.4.1. Macroscopic ordering

Special arrangements of zeolite crystals containing guest species constitute another hierarchy of structural order and are important for the development of specific applications. We will in the following focus on the arrangement of preformed zeolite crystals. For a recent review on membranes and films of zeolite materials see Ref. [51]. Growth of uniformly aligned silicalite-1 crystals on glass with the *a*- or *c*-axes of the crystals oriented perpendicular to the substrate was recently achieved by Yoon and coworkers [52] through the use of polyurethane films as matrices.

One of the first methods for postsynthetic orientation of zeolite crystals was developed by Caro et al. [53]. They observed that crystals of $AlPO_4$-5 and ZSM-5 can be oriented in a parallel alignment upon application of an electric field of 2–3 $kV\,cm^{-1}$. However, crystals larger than 20 μm and aspect ratios of at least four to five are required for a successful alignment. Large ZSM-5 crystals (several tenths of μm) of uniform size can also be aligned in the grooves of etched silicon wafers, as shown by Scandella et al. [54]. High quality close-packed monolayers of size-selected zeolite A crystals ranging from 2 to 8 μm were prepared by sedimentation [2]. This method can be applied to various substrates and extended to other types of zeolites. Covalent bonding between zeolite (LTA, ZSM-5) and substrate (usually glass) using a variety of linking molecules was studied by Yoon and coworkers [3]. The principles of covalently anchoring zeolites were used by the same group to produce micropatterned monolayers of ZSM-5 [4]. We are currently investigating possibilities to generate robust monolayers of zeolite L crystals having the channels perpendicular to the surface of the substrate. Subsequent insertion of dye molecules into the open channel end is expected to result in systems where excitation energy is transported in one direction only (see Fig. 12). Such a monodirectional photonic antenna is desirable for coupling to an external macroscopic device, e.g., a semiconductor (see Section 2.4.2). Moreover, highly ordered systems with non-linear optical properties can be obtained if a non-centrosymmetric dye is inserted in its preferred orientation [55].

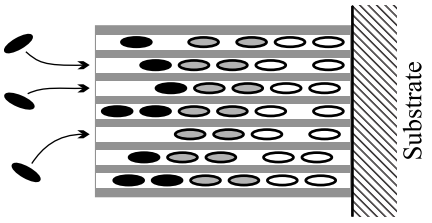

Fig. 12. Strategy for synthesizing monodirectional photonic antennae. Attachment of the base of the zeolite L crystals to a substrate allows filling of the channels from one side only.

2.4.2. Coupling to external devices

In view of practical applications the coupling of dye–zeolite composites to external devices is of special interest. The coupling of bidirectional antennae (see Fig. 10) to a luminescent or photoconductive polymer offers possibilities for the development of novel LED materials [24]. When embedding zeolite crystals in polymer films, methods to covalently anchor dye molecules on the outer surface of the zeolite can be employed to enhance the contact area between polymer and zeolite. Such grafting procedures which use silane reagents to couple the dyes to the surface of the crystals have been applied to immobilize dye molecules in mesoporous silica (see Section 4). We have recently prepared a polymer embedded, surface modified Ox^+–zeolite L, for which we observed transfer of electronic excitation energy from the photoconductive polymer to the dye molecules at the external zeolite surface and ultimately to the Ox^+ molecules located in the channels [56a]. Energy transfer from dye–zeolite crystals to bulk silicon has also been demonstrated [56b].

In 1979 Dexter proposed a dye-sensitized solar cell which employs energy transfer instead of electron injection [57]. The advantage of such a cell is that the dyes do not require regeneration. This is in contrast to cells working by electron injection, in which the dyes have to be regenerated by a redox couple. A dye–zeolite composite prepared as a monodirectional antenna would open possibilities for novel sensitized solar cells. Arranging small composite crystals with their *c*-axes perpendicular to the surface of a semiconductor would allow transport of the excitation energy towards the zeolite–semiconductor interface by energy migration. Stopcock molecules are placed at the channel ends to allow energy transfer. Only a very thin semiconductor is needed in this case, because the electron–hole pairs form near the surface. The transfer of electrons from antenna to semiconductor can be prevented by introducing an insulating layer [5]. Energy can also be transferred from the semiconductor to the antenna composites by reversing the current and putting a voltage over the semiconductor. The dye–zeolite composites on the semiconductor surface subsequently lose their energy by emitting light. The color of the emission can be tuned by

adapting the ratio of blue, yellow, and red fluorescent dyes. Higher luminescence efficiency is expected for such a system compared to conventional LEDs [5].

3. Supramolecular organization of metal sulfide particles in zeolites

3.1. Introduction

Semiconductor particles in the nanometer size regime are considered as potential building blocks for molecular electronics and photonics [58,59]. An important characteristic of nanosized particles is their tunable properties due to quantum confinement effects QCE (e.g., band gap depending on particle size) [60]. Significant QCE could be observed in metal sulfide clusters such as CdS [61], ZnS [62], and PbS [63]. The synthesis of small clusters of these materials is often complicated by their tendency to form larger aggregates. By using a host with a defined and robust cage structure, the particle growth can be controlled and limited. The pioneering work on the use of zeolites as host materials for the inclusion of metal sulfide clusters was conducted by Herron et al. [64] with the preparation of cubane-like $(CdS,O)_4$ clusters located in the sodalite subunits of zeolite Y. The electronic absorption spectrum of the CdS–zeolite composites was found to strongly depend on the CdS loading. Increasing the loading level shifted the 280 nm absorption observed for low CdS content to the red. It was suggested that this effect is due to the interaction of isolated clusters resulting in an extended electronic structure modulated by the zeolite framework [65]. While quantum cluster calculations complement and confirm the above results [66], other research groups have made observations not supporting these conclusions. Liu and Thomas [67] investigated the formation of CdS clusters in zeolites A, X, L, ZSM-5, chabazite, offretite, and sodalite. Contrary to the observations of Herron et al., they found that CdS clusters always form in the large cavities of a given zeolite (e.g., α-cage in zeolite A, supercage in zeolite X). It was further suggested that in cases where the amount of Cd^{2+} cations in the large cages is not sufficient, Cd^{2+} located in the small cages can migrate to the larger cavities and thus become available for CdS cluster formation. A recent positron annihilation study on CdS in zeolite Y indicates that the clusters are located in the sodalite cages [68] and are therefore in agreement with the results of Herron et al. It has to be noted that most of the studies on CdS–zeolite composites use slightly different preparation procedures and, not less importantly, zeolite materials of different quality and origin. It is very likely that these factors affect the properties of the final product. Wark et al. [69] found that the usual synthesis procedure, namely ion exchange of Cd^{2+} followed by exposure to H_2S, can lead to fragmentation of the zeolite X framework initiated by the growing sulfide particles and by the protons liberated from H_2S, yielding clusters with sizes up to 10 nm located in mesopores. This effect is probably of increasing importance with decreasing Si/Al ratio. It can thus be expected that the extent of fragmentation of the zeolite X framework upon sulfidation is larger than for zeolite Y. In addition to affecting the integrity of the zeolite framework, the protons liberated upon reaction of Cd^{2+} and H_2S are also problematic in terms of generating an extremely acidic environment in which the CdS clusters are forced to reside. The stability of CdS in such an environment is limited and evacuation of a CdS–zeolite sample readily caused dissociation of CdS into Cd^{2+} and H_2S thereby reversing the CdS formation [64]. We have found that such a problem does not occur in the case of silver sulfide clusters in zeolite. The reason for this different behavior can be attributed to the much higher stability of Ag_2S in acidic environments [70].

An important factor, often overlooked, is the history of a given cluster–zeolite sample. CdS–zeolite composites must be stored and handled in dry atmosphere to avoid adsorption of water (atmospheric moisture) which initiates migration and aggregation of the discrete CdS clusters [64]. If comparisons between different cluster–zeolite samples need to be drawn, the postsynthetic handling of the samples should follow a standard procedure.

The approach used for the synthesis of CdS clusters in zeolites can be applied to other sulfides. Moller et al. [71] prepared small clusters of PbS in zeolite Y and mordenite and found that Pb^{2+} is anchored to the zeolite framework while being simultaneously coordinated to two sulfur atoms. No red shift of the electronic absorption was observed upon increasing the PbS loading. In combination with EXAFS data it was concluded that PbS exists mostly as molecular species in zeolite Y. Superstructures as postulated for CdS could therefore not be observed. The method of ion exchange and subsequent sulfidation has also been used to generate MnS [72] and Ga_2S_3 clusters [73]. Bowes and Ozin [74] employed a different strategy for the synthesis of tin sulfide clusters in zeolite Y. The reaction of tetramethyltin with H_2S was found to form charge-balancing clusters of average $Sn_4S_6^{4+}$ stoichiometry located in the supercages of the zeolite. Using $Mo(CO)_6$ and $Co(CO)_3NO$ as precursors, Okamoto et al. [75] synthesized $Co_2Mo_2S_6$ clusters in zeolite Y and proposed a thiocubane structure within the supercage.

Aggregation is a particular problem in the synthesis of small silver sulfide clusters. Stabilization of particles with diameters ranging from 20 to 150 Å was in this case achieved through inclusion into reverse micelles [76], nylon thin films [77], nafion membranes [78], silica glass [79], hyperbranched polyurethane matrices [80], through

capping with suitable molecules [81] or upon reaction of Na_2S with silver(I)-thiolate polymers [82]. The size regime below 20 Å becomes accessible by synthesizing silver sulfide clusters within the α-cages of zeolite A through exposure of the activated Ag^+-exchanged zeolite to H_2S [31]. Silver sulfide particles of such small size are believed to play an important role in photographic sensitivity [83]. In the following chapter we will describe the different stages of silver sulfide cluster synthesis, taking Ag^+-exchanged zeolite A and its unique properties as starting point. We will further illustrate the essential role of the zeolite in the cluster formation process. Finally, Section 3.3 is devoted to the discussion of the remarkable optical—especially photoluminescence—properties of the $(Ag_2S)_n$–zeolite composites.

3.2. From silver ions to silver sulfide clusters

3.2.1. Silver ions in zeolite A

The first step in our silver sulfide cluster synthesis is the loading of the zeolite with Ag^+ by ion exchange from aqueous solution. Eight 6-rings, three 8-rings, and 18 4-rings are present in a pseudo unit cell of zeolite A to coordinate the cations. It is well-known that the affinity of a cation towards a specific coordination site depends primarily on its size, with small ions (Na^+, Ca^{2+}, Ag^+) preferring 8-ring sites. This selectivity towards different coordination sites is the origin of a phenomenon first reported by Rálek et al. in 1962 [84]. It was found that Ag^+-loaded sodium zeolite A ($Ag_x^+Na_{12-x}^+A$) turns yellow to red on activation, while the same material is colorless in its hydrated state. This effect was later attributed to the formation of intrazeolitic silver clusters (Ag_n^0) through an autoreduction process at elevated temperature [85]. In contrast, our recent observation that room temperature activation under high vacuum is sufficient to reversibly yield the yellow form of $Ag_x^+Na_{12-x}^+A$ proved a dependence on the hydration state. Upon activation the silver ions are forced to coordinate to framework oxygen atoms because the number of water molecules available for coordination decreases. The yellow color was therefore assigned to electronic charge transfer transitions from the oxygen lone pairs of the zeolite framework to the empty 5s orbitals of the silver ions [86]. A similar effect has been observed for Cu^+ in zeolites A and X [87,88].

Fig. 13 shows the diffuse reflectance spectra of hydrated and room temperature activated $Ag_6^+Na_6^+A$. No absorption bands were found in the investigated range for pure sodium zeolite A. The spectrum of the fully hydrated sample matches that of an aqueous silver perchlorate solution. The band at 220 nm is therefore attributed to a charge transfer transition from H_2O (coordinated to Ag^+) to the empty 5s state of Ag^+. Room temperature activation in high vacuum leads to new bands, most notably an absorption around 450 nm

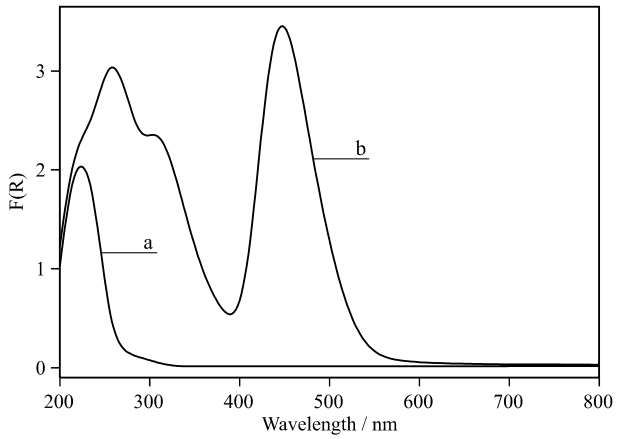

Fig. 13. Diffuse reflectance spectra of freshly exchanged $Ag_6^+Na_6^+A$ before activation (spectrum a) and after activation under high vacuum at room temperature (spectrum b). Rehydration by exposure to water vapor restores spectrum a [86]. Pure sodium zeolite A shows no absorption in the investigated spectral range.

which is responsible for the yellow color of the material. The fact that this band can be observed for loadings below $x = 0.2$ indicates that isolated Ag^+ are sufficient to produce it. Rehydration completely reverses the spectral changes [86,89]. A red coloration was obtained upon activation at elevated temperature for yellow samples with loadings of $x > 1$.

The question whether specific coordination sites act as yellow and/or red color centers was investigated by comparing the UV–Vis spectra of hydrated and activated $Ag_x^+Na_{12-x}^+A$, $Ag_x^+Ca_{6-0.5x}^{2+}A$, and $Ag_{9.5}^+ZK\text{-}4$ materials. A general model describing the distribution of independent particles in microporous materials [90] has been employed for interpreting the spectra in function of the exchange degree x [86]. In conjunction with gas adsorption experiments and molecular orbital calculations of a unit structure cell consisting of 1296 atoms, the results clearly indicated that 4-ring coordinated Ag^+ is responsible for the yellow color observed upon activation, while the red color (only obtained upon heating in high vacuum) is due to the interaction of Ag^+ at 4-ring sites with Ag^+ at adjacent 6-ring sites [89]. The reversibility of the room temperature activation of Ag^+-loaded zeolite A and the absence of autoreduction processes opened the way for a size-controlled silver sulfide cluster synthesis through reaction with H_2S.

3.2.2. Silver sulfide cluster growth

Exposure of dehydrated Ag^+-loaded zeolite A to H_2S first leads to the formation of AgSH molecules with the silver center partially coordinated to framework oxygen atoms. Adsorption of water increases the mobility of the AgSH molecules. This effect is analogous to the mobilization of organic dye molecules in zeolite L upon adsorption of water (see Section 2.2.1). Encounter of

two AgSH molecules then generates Ag_2S and H_2S, the latter being liberated from the zeolite [31b]. Compared to AgSH, diffusion of Ag_2S is expected to occur at a slower rate due to sterical hindrance. However, further cluster growth is still possible through addition of AgSH molecules to Ag_2S. Thermal treatment stimulates the cluster growth [32]. The silver sulfide content, which is controlled by adjusting the initial Ag^+ loading, determines the size of the clusters. Monomers of Ag_2S are obtained at low initial Ag^+ content, while Ag_4S_2 is increasingly favored at higher Ag^+ content. The structure of clusters larger than the Ag_2S monomer is to date not known. Quantum chemical calculations suggest that a variety of energetically favorable geometries are possible already for Ag_4S_2 [91].

The intrazeolitic $(Ag_2S)_n$ particles show a high stability under ambient conditions which may in part be attributable to the extremely low solubility of silver sulfide in water [70]. Decomposition of the zeolite host by treatment with hydrochloric acid leads to instant aggregation of the silver sulfide species yielding black particles which exhibit properties of bulk α-Ag_2S, i.e., monoclinic structure [92] and a band gap around 1 eV [93]. It becomes evident from this observation that the zeolite does not only provide a template for the spatial organization of the guest compound but also acts as a stabilizing agent.

The preparation of $(Ag_2S)_n$–zeolite composites is an example of a ship-in-a-bottle synthesis. While for low loading levels this approach usually results in a homogeneous distribution over the whole zeolite framework, care must be taken with high loadings where the formation of products (e.g., large metal sulfide clusters) in cavities close to the outer surface of the zeolite can inhibit the diffusion of educt molecules to the inner part of the crystals. High loading levels can additionally lead to the destruction of the zeolite framework due to the large amounts of protons liberated during the reaction of Ag^+ with H_2S. While the latter effect has also been observed in the case of CdS clusters in zeolite X [69], the effect of a heterogeneous product distribution has been investigated in detail for the inclusion of tris(2,2′-bipyridine)ruthenium(II), $Ru(bpy)_3^{2+}$, into the supercages of zeolite Y. The synthesis of these ship-in-a-bottle complexes pioneered by Lunsford and coworkers [94] was found to yield a homogeneous distribution only for loading levels below 65% (two complexes per three supercages) [95]. At higher loading, complexes are first formed at sites close to the outer surface, thereby causing pore blockage and preventing bpy molecules from reaching the inner part of the zeolite crystals.

3.3. Properties of silver sulfide clusters in zeolite A

3.3.1. Theoretical considerations

The $(Ag_2S)_n$–zeolite system constitutes a three-dimensional cluster array. The question arises whether the properties of this system are governed by crystal effects originating from interacting clusters. We evaluated the relevance of such effects by calculating the density of states (DOS) of Ag_4S_2 clusters arranged in a cubic lattice [31b]. The development of the DOS upon variation of the lattice constant is shown in Fig. 14. Significant changes, such as a decrease of the band gap, were found only when the lattice constant was set to values below 10 Å. Taking into account that the distance between the centers of two α-cages in zeolite A is 12.3 Å [96], the model excludes through space interaction between the clusters over the whole zeolite crystal. Up to a loading of 4 Ag^+ per α-cage, the properties of the material are therefore mainly determined by the presence of isolated clusters and by short-range interactions.

3.3.2. Photoluminescence

The optical properties of the $(Ag_2S)_n$–zeolite composites strongly depend on the silver sulfide content (see Figs. 15 and 16). Photoluminescence spectra typically feature two bands, one around 480 nm (blue-green

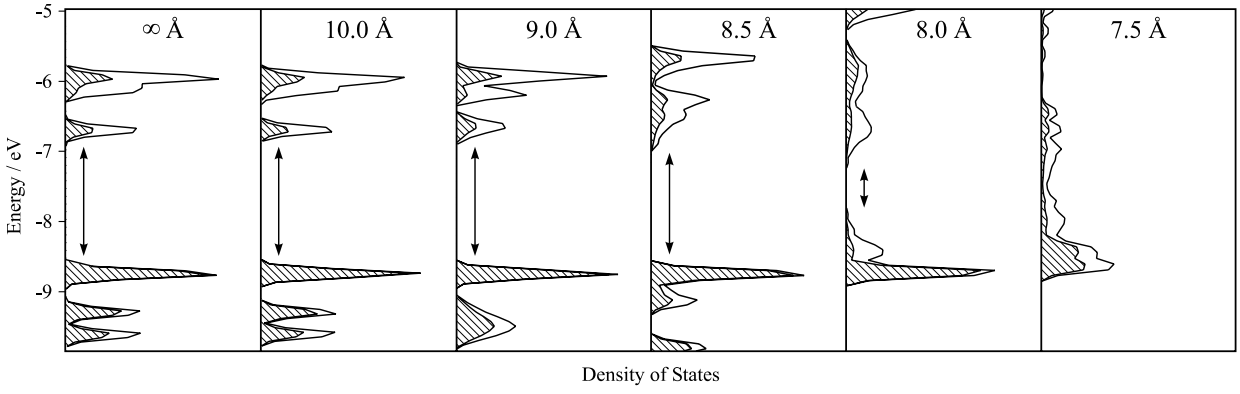

Fig. 14. Density of states (DOS) of Ag_4S_2 clusters in a cubic lattice with different lattice constants. The band gap for each cluster array is marked by an arrow. The hatched region indicates the contribution of sulfur states [31b].

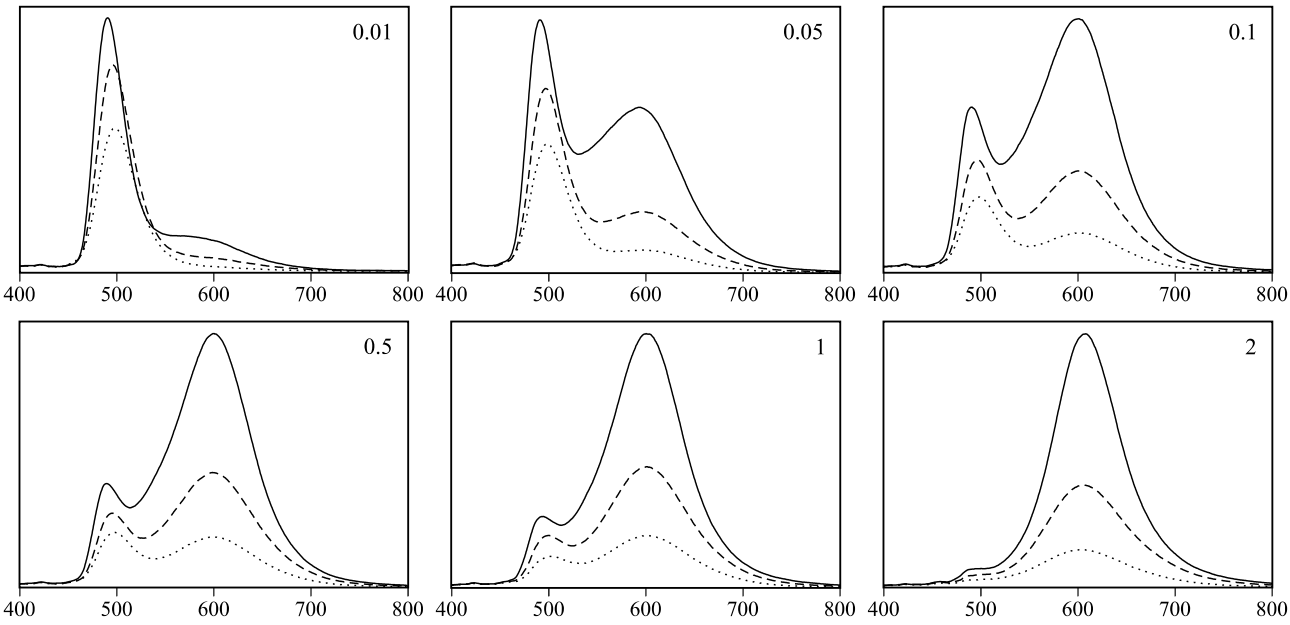

Fig. 15. Luminescence spectra of silver sulfide in calcium zeolite A at −195 °C (—), −100 °C (– – –) and −50 °C (···). The abscissa and the ordinate give the wavelength in nanometers and the emission intensity, respectively. The spectra are labeled with the corresponding average number of Ag^+ per α-cage. Excitation was performed at 280 nm [31b].

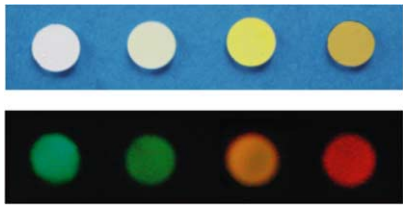

Fig. 16. Photographic pictures of zeolite A containing silver sulfide with increasing silver sulfide content from left to right. Top: Color seen in reflection. Bottom: Luminescence of the same samples at −10 °C upon excitation at 360 nm [32].

emission), and the other at 600 nm (orange-red emission). While the former is observed in samples with low silver sulfide loading, the latter increasingly dominates the spectra at higher silver sulfide content (see Fig. 15) [31]. In conjunction with their characteristic excitation spectra, the luminescence bands were assigned to Ag_2S monomers (blue-green emission) and Ag_4S_2 (orange-red emission). Energy transfer of the Förster type between Ag_2S (donor) and Ag_4S_2 (acceptor) was proposed for samples containing both species [32].

Another interesting property of the luminescence of $(Ag_2S)_n$–zeolite A composites is the distinct temperature dependence extending over a considerable range (80 K and below to room temperature). Unequal thermal quenching was observed for the two prominent luminescence bands, the orange-red emission showing stronger quenching with increasing temperature. Such samples could be employed in thermometry applications by observing the luminescence color and intensity, the luminescence lifetimes, and the intensity ratio of the Ag_2S (blue-green) and Ag_4S_2 (orange-red) emissions. An advantage of a thermometer built from $(Ag_2S)_n$–zeolite composites is that a contact with an electric device is not required. Making use of the fact that the zeolite crystals can be arranged in monolayers [2,3] and in defined micropatterns [4] would furthermore open possibilities to map surface temperatures with high spatial resolution.

4. Supramolecular organization in materials of the M41S family

4.1. Introduction

The discovery of the periodic mesoporous molecular sieves of the M41S family by researchers at Mobil in 1992 [97] was rapidly followed by a variety of reports on the inclusion chemistry of these materials [98], even initiating research on the immobilization of enzymes [99], thereby considerably widening the scope of supramolecular organization in molecular sieves. We will in this section mainly focus on the use of siliceous MCM-41 (one-dimensional, hexagonally ordered pore structure) and MCM-48 (three-dimensional, cubic ordered pore structure) as host material and highlight some features essential for the organization of guest species.

The most important functionality of the M41S materials with respect to inclusion chemistry is the surface silanol group. Fig. 17 shows the three types generally distinguished [100,101]. At elevated temperatures,

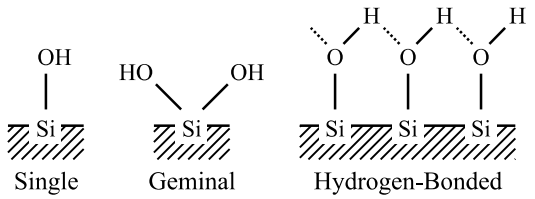

Fig. 17. Schematic representation of the three types of silanol groups in M41S materials.

dehydroxylation of hydrogen-bonded and geminal silanol groups occurs under formation of siloxane bonds. Simultaneously more single silanol groups are generated. Zhao et al. [100] determined the number of silanol groups of MCM-41 by means of NMR and found 2.5 to 3.0 silanols per nm^2. The silanol groups are not acidic and Brønsted-acid bridging OH groups are formed only after modification with aluminum [101]. Free silanol groups (single and geminal) are highly accessible to the silylating agent chlorotrimethylsilane and therefore provide a convenient target for modification. Covalent bonding of guest species to these groups prevents leaching and/or aggregation, which is a common problem in mesoporous materials. As will be shown in Section 4.3, silanol groups also act as ligands and can therefore be employed to immobilize metal complexes.

Although the pore walls of MCM-41 and MCM-48 are generally considered amorphous, a distinction should be made between long-range, medium-range, and short-range order, the latter being represented by the local coordination polyhedra. While the pore walls do not feature any long-range order, a considerable degree of medium-range order (within 8 Å) was proposed for MCM-41 by Pophal and Fuess [102]. It is very likely that such well-defined regions on the internal surface provide suitable adsorption and grafting sites.

4.2. Inclusion of organic dyes in M41S materials

The separate steps of covalently anchoring a dye molecule on the pore surface of a M41S material is illustrated by a recent example (see Fig. 18) [103]: In a first step the external surface of the host material must

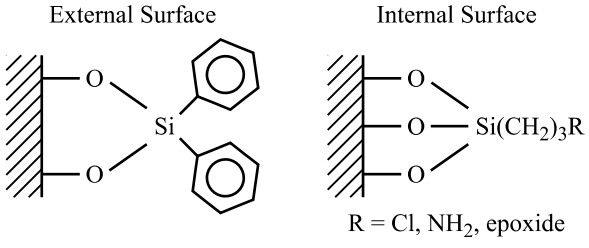

Fig. 18. Modification of the external and internal surface of M41S materials allowing the covalent attachment of guest molecules inside the pores. The guest to be grafted has to provide a moiety able to react with the surface group R (e.g., isothiocyanate for $R = NH_2$).

be passivated, which is efficiently achieved by reaction with dichlorodiphenylsilane [104]. Exposure to 3-aminopropyltriethoxysilane then leads to a selective modification of the internal surface with aminopropyl moieties. Fluorescein isothiocyanate (FITC) can ultimately be attached to the pore walls through reaction of the isothiocyanate group of the dye with the surface anchored amino groups. Rhodamine B and phthalocyanines have been grafted to the internal surface of MCM-41 by similar methods, thereby demonstrating the ability of M41S materials to accommodate and immobilize bulky dye molecules [105]. Dyes grafted by the above method cannot be removed by Soxhlet extraction. Covalent anchoring of dye molecules is also possible during the synthesis of the mesoporous material by co-condensation of silane functionalized dye molecules with tetraethoxysilane [106–108]. Wark et al. [107] found that rhodamines anchored in the pores of MCM-41 can be used to detect SO_2 by observing the quenching of the dye's fluorescence. The level of organization of dye molecules anchored to the pore walls of mesoporous silica is lower compared to the dye–zeolite composites described in Section 2, i.e., alignment of electronic transition moments in dye-loaded MCM-41 is usually not observed. The significant feature, however, is the larger pore diameter of the mesoporous host, which allows incorporation of almost any dye molecule. For a recent review see Ref. [6].

Kinski et al. [109] investigated the inclusion of *para*-nitroaniline (*p*NA) into MCM-41 and found different crystallographically ordered arrangements which were strongly influenced by the loading procedure and by co-adsorbates. Samples that were aged in air for several weeks after introducing *p*NA from the gas phase showed an increasing second harmonic generation signal, indicating polar alignment of the *p*NA molecules within the channels.

A second stage of organization in the sense of a selective closure of the channel entrances was accomplished for MCM-41: Using the photocontrolled and reversible intermolecular dimerization of coumarin derivatives attached to the pore outlets, Mal et al. [110] were able to control the uptake, storage, and release of organic molecules. Access to the interior of MCM-41 is possible when the coumarin substituents at the channel entrances are present as monomers. Irradiation in the UV with wavelengths longer than 310 nm induces photodimerization, hence resulting in cyclobutane dimers spanning the entrances and obstructing access. Photocleavage of the coumarin dimers and therefore reopening of the channels is accomplished by irradiation at 250 nm. Successful functionalization required as-synthesized MCM-41, i.e., MCM-41 filled with template molecules, to ensure preferential adsorption of the coumarin derivatives at the channel entrances. Controlled release of guest molecules by chemical triggering was achieved

by Lai et al. [111] using CdS nanocrystals as removable caps at the channel entrances. The resulting material is promising for the development of new devices for controlled drug delivery. Contrary to MCM-41 or zeolite L, the closure of pore openings is usually less effective in molecular sieves possessing interconnected channel systems, where just a few open pores can provide access to the whole channel network.

4.3. Isolated transition metal centers in M41S materials

4.3.1. General concepts

The functionalization of the internal surface of M41S materials with silane reagents [112] not only allows the immobilization of organic molecules, but similarly opens possibilities for anchoring organometallic complexes. There are several recent reviews on this topic: Brunel et al. [113] and Anwander [114] describe advanced synthetic concepts of surface organometallic chemistry at periodic mesoporous silica. Jacobs and coworkers [115] and Corma [116] discuss the possibilities of transition metal functionalized microporous and mesoporous molecular sieves as catalysts for selective organic transformations.

Two general approaches for introducing isolated transition metal centers into mesoporous silica can be distinguished: (1) framework substitution (''one-pot synthesis'') and (2) postsynthetic methods. In the following we will discuss these methods in detail and emphasize those employing surface silanol groups as ligands, leading to grafted complexes with at least one Si–O(H)–M bridge (M = metal). Besides being of interest for catalytic applications [116], such materials have also been observed to possess photocatalytic abilities. Anpo et al. [117] showed that highly dispersed tetrahedral Ti^{4+} centers in MCM-41 and MCM-48 can be used to photoreduce CO_2 with H_2O to CH_4 and CH_3OH. The long-lived excited charge transfer state $(Ti^{3+}–O^-)^*$ formed under UV irradiation initiates the reaction. The photocatalytic reactivity of Ti-containing mesoporous silica was significantly higher compared to bulk TiO_2. Similarly, photocatalytic reactivity for the decomposition of NO_x was observed for MCM-41 containing dispersed tetrahedral Mo^{6+} [118].

4.3.2. Framework substitution

In the framework (isomorphous) substitution method, metals are introduced during the hydrothermal synthesis of the sieve and subsequently become part of its wall structure. This approach has strong limitations concerning the size of the metal atom, selection of the oxidation state, or restriction to low metal concentrations (usually 1–2 mol%), and has mainly been applied for the inclusion of d^0 transition metals such as Ti^{4+} [119], Zr^{4+} [120], V^{5+} [121], Nb^{5+} [122], and Mo^{6+} [122]. Metals of lower oxidation state are generally oxidized during calcination. This has been observed for Cr^{3+} (oxidized to Cr^{6+}), Mn^{2+} (oxidized to Mn^{5+}), and Co^{2+} (oxidized to Co^{3+}) [123]. Incorporation into the MCM-41 structure by a ''one-pot synthesis'' approach has also been reported for Cu^{2+} and Fe^{3+} [122]. Synthesis parameters have to be adjusted carefully to avoid the formation of extra-framework metal oxide phases.

4.3.3. Postsynthetic modification

Postsynthetic methods employ the reaction of preformed mesoporous silica with suitable transition metal complexes. The mesoporous material can be in its as-synthesized state (still containing the template) [124], but usually calcination or solvent extraction is performed before incorporation of the transition metal. The metal complexes are either directly grafted to the surface using surface silanols as ligands (primary modification) or grafted onto a previously functionalized surface (secondary modification) [125]. Compared to framework substitution, these methods provide a better control over the coordination sphere and the oxidation state of the metal.

The potential of the primary modification method was impressively demonstrated by Thomas and coworkers [126] with their synthesis of Ti^{4+} modified MCM-41 containing highly dispersed, isolated tetrahedral titanium centers. The use of titanocene as precursor was found to reduce to amount of oligomeric TiO_2 species, therefore being superior to $TiCl_4$ or $Ti(OR)_4$ precursors. It was proposed that titanocene first forms a tripodal complex by substitution of one cyclopentadienyl (cp) ligand with three surface silanols. The remaining cp ligand thereby protects the Ti center preventing the formation of Ti–O–Ti bridges. Calcination in oxygen at 550 °C removes the cp ligand and a structure as shown in Fig. 19 results. The superior catalytic performance of

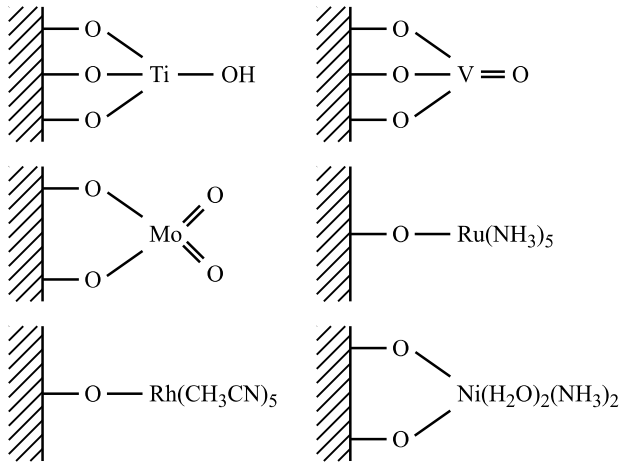

Fig. 19. Structure of grafted transition metal complexes on mesoporous silica via oxo-bridges. From top left: Ti^{4+} [126], V^{5+} [129], Mo^{6+} [131], Ru^{3+} [134], Rh^{2+} [135], and Ni^{2+} [134]. The first three complexes adopt a tetrahedral configuration, the others are octahedral.

grafted versus framework substituted Ti-MCM-41 has been demonstrated for the epoxidation of alkenes [127].

Employing the surface silanol groups as ligands has opened possibilities to achieve site isolated oxo-bridged grafting not only for Ti, but also for Zr [128], V [129], Cr [130], Mo [131,132], W [132], Fe [133], Ru [134], Rh [135], and Ni [134], as well as rare earth metals [136]. A selection of structures is shown in Fig. 19. In contrast to transition metal molecular sieves obtained by framework substitution, materials prepared by postsynthetic grafting still constitute host–guest systems, whereby the host acts as a large polydentate ligand. Based on their studies of the adsorption of nickel complexes on amorphous silica, Che and coworkers [137] suggested that surface groups can be treated as ligands in the classical sense and proposed the classification of the surface siloxy group within the spectrochemical series. As a result, the siloxy group can be placed close to H_2O with the tendency of being a slightly weaker ligand. This general trend is most probably applicable to mesoporous silica as well, although the exact effect of a given surface group on the crystal field stabilization energy will to certain extent also depend on the properties of the surface (environment of the group, degree of protonation). Understanding the influence of a surface group on the d-d transitions of a metal can be practical for identifying the podality of a grafted complex by means of UV–Vis–NIR spectroscopy.

Although the pore walls of M41S materials can be considered amorphous, i.e., not possessing long-range order, the reactivity of the silanol groups does not necessarily compare to those of common amorphous silica such as Aerosil. One specialty of MCM-41 is the uniformly concave internal surface. The silanol groups are therefore pointing to convergent directions, while the opposite is the case for the convex surface of Aerosil silica [138]. Experimental evidence for the different reactivity of MCM-41 and amorphous silica was obtained in the grafting of Ni^{2+} ammine complexes. While the formation of nickel silicates (phyllosilicates) was observed in the case of the amorphous silica [139], isolated nickel centers resulted upon grafting onto the pore surface of MCM-41 [134]. This effect was in part attributed to the compartmentalization of the internal surface of MCM-41 by the one-dimensional channel system, which severely restricts the overall mobility of the complexes. Agglomeration by formation of Ni–O–Ni bonds is therefore less likely inside the pores of MCM-41 than on the open surface of amorphous silica. The importance of the high level of organization provided by the MCM-41 support was also observed by Balkus and coworkers [140], who functionalized the pore surface with ethylenediamine, diethylenetriamine, and ethylenediaminetriacetic acid sites. These grafted ligands were found to readily bind Co^{2+}. The uniform pore structure of MCM-41 thereby supported limited coordination of cobalt to adjacent ligands. Amorphous silica, on the other hand, possesses a wide pore size distribution, which would enable many more coordination modes. It is important that such beneficial effects of the mesoporous structure are identified, considering that less costly high surface area supports, e.g., silica gels, might be just as well suited to accomplish a given task.

The observation that well-defined structures of transition metal complexes are obtained by postsynthetic grafting is astonishing considering the amorphous nature of the pore surface. Recent investigations on the adsorption of Ni^{2+} polyamine complexes on amorphous silica lead to the conclusion that molecular recognition phenomena might play an important role in the grafting process [141]. It was suggested that Ni^{2+} polyamine complexes recognize well-defined local surface configurations through the formation of hydrogen bonds before ligand substitution by silanol groups occurs. It is very likely that such an effect is operative in the case of M41S materials as well: Grafting of Ni^{2+} ammine complexes onto the pore surface of MCM-41 resulted in a dipodal structure which was readily converted into a strained tripodal geometry upon dehydration (see Fig. 20). The additional link to a surface silanol was immediately broken upon rehydration or exposure to NH_3. Hydrogen bonding between ammine ligands and surface groups was found to be essential for the stabilization of the grafted complexes [134].

Consecutive grafting of different metals onto the same mesoporous silica or the combination of isomorphous substitution and subsequent grafting allows for the synthesis of bimetallic composites possessing the well-defined pore structure provided by the support [134,142]. The modification of a molecular sieve with more than one transition metal not only offers new ways of tuning its catalytic properties but is also of interest for photochemical applications. Transition metal molecular sieves have been used for a variety of transformations employing the isolated metal oxides as photoredox centers [117,143]. The possibility of combining different photoredox centers or connecting them by bridging ligands while one of the centers remains grafted to the pore surface opens possibilities to achieve higher yields and/or selectivities, while simultaneously allowing a

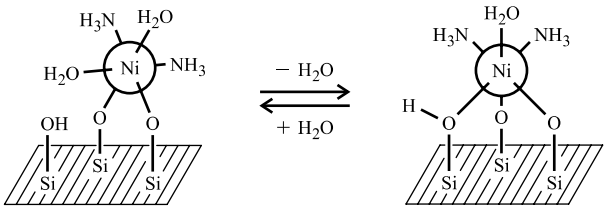

Fig. 20. Structure of a Ni^{2+} aquoammine complex grafted to the pore surface of MCM-41. Dehydration under high vacuum converts the dipodal into a strained tripodal configuration through an additional link to a surface group [134].

systematic tuning of the light absorption properties of the photocatalyst.

5. Summary and outlook

The use of molecular sieves as host materials for supramolecular organization allows for choosing from a variety of framework topologies. Yet, as noted by Behrens and Stucky in their review on novel materials based on zeolites [144], a large percentage of guest–zeolite composites have been prepared on the basis of only three framework types, namely the popular LTA, FAU, and MFI [145]. Our research on dye–LTL composites described in Section 2 is a notable exception. In order to make more use of the structural diversity, framework types should not be selected in terms of their popularity, but rather in terms of their potential to provide optimum performance for a desired application. It is evident that mesoporous materials, most prominently the members of the M41S family, complement zeolites as hosts by offering new possibilities to accommodate larger guests and by exhibiting a unique chemistry associated with the surface silanol groups. Further understanding of the pore wall structure and reactivity of M41S materials will be beneficial in developing new techniques for organizing guest species. Optimum use of a molecular sieve as host material requires profound knowledge of its properties. Since the discovery of MCM-41, the understanding of mesoporous silica has advanced considerably [6,98,146], in great part due to the investigation of inclusion compounds. Nonetheless, more work needs to be done in order to achieve the current level of understanding associated with the most common zeolites. The comparison to systems using different hosts, e.g., clay minerals [147] or organic hosts such as perhydrotriphenylene (PHTP) [148], can thereby serve as a valuable tool.

A great variety of novel materials, especially in the field of quantum dots and wires, has resulted from the synthesis of guest species in porous materials [144]. As shown by our studies on the formation of silver sulfide clusters in zeolite A, the cavities of molecular sieves can be used as reaction vessels to control chemical transformations and particle growth. In any case where zeolites are used as host materials, water has to be considered an important factor. This also holds for materials of the M41S family, which, due to their strongly hydroxylated internal surface, behave hydrophilic [101]. While the effects of water on a guest–zeolite composite can be diverse, the increased mobility of guest species upon hydration of the zeolite is the most common characteristic. For guests featuring only a weak interaction with the zeolite (e.g., molecules without polar groups), liberation of the included species upon hydration is often observed. The selective closure of channel entrances, which has been achieved for zeolite L [48] and MCM-41 [110], provides means of controlling this phenomenon. Changes of the hydration level can also affect the growth of intracavity particles (see Section 3.2.2) or initiate grafting reactions [134].

The potential applications of the materials discussed in this review are manifold. For dye–zeolite composites, possible applications ranging from pigments to dye-sensitized solar cells and LEDs have been summarized in Ref. [5]. While semiconductor clusters in zeolites continue to attract interest due to their intriguing properties such as quantum-size effects, much further development is required to achieve the ultimate goal of creating optoelectronic devices. Achieving a uniform cluster size homogeneously distributed over the three-dimensional framework of a given zeolite is the major problem. Semiconductor–zeolite based applications such as gas sensing [107] or thermometry, which do not rely on the high level of organization required for optoelectronic devices, seem to be more feasible. As for mesoporous solids, there is to our knowledge no commercial process or product using these materials to date. In many cases, especially when it comes to catalysis, the performance of a given mesoporous solid needs to be significantly better compared to a system using a less costly material featuring a lower degree of organization. A crucial advantage of mesoporous materials, however, is their very high surface areas and the effect of the defined pore structure on the specificity of reactions (e.g., site isolated grafting) and organization of guest species.

The coupling of molecular sieve based host–guest composites to external devices is essential for fully exploiting their potential. The successful design of interfaces which allow the communication between the composite and external components requires a level of organization beyond the arrangement of the incorporated guest species. The realization of devices consisting of guest–sieve assemblies interacting with other components constitutes a challenging field of research in which considerable progress can be expected in the near future.

Acknowledgements

Financial support by the Swiss National Science Foundation (Project NFP 47, 4047-057481) is acknowledged. The authors also thank the Bundesamt für Bildung und Wissenschaft (BBW Switzerland) for financial support within the European Union Project 'RTN Nanochannel'. The data reported in Fig. 7 was measured by Roman Bolliger.

References

[1] (a) Y. Yan, T. Bein, J. Phys. Chem. 96 (1992) 9387;
(b) T. Bein, Chem. Mater. 8 (1996) 1636;

(c) A.R. Pradhan, M.A. Macnaughtan, D. Raftery, J. Am. Chem. Soc. 122 (2000) 404.
[2] P. Lainé, R. Seifert, R. Giovanoli, G. Calzaferri, New J. Chem. 21 (1997) 453.
[3] (a) S.Y. Choi, Y.-J. Lee, Y.S. Park, K. Ha, K.B. Yoon, J. Am. Chem. Soc. 122 (2000) 5201;
(b) K. Ha, Y.-J. Lee, H.J. Lee, K.B. Yoon, Adv. Mater. 12 (2000) 1114;
(c) A. Kulak, Y.-J. Lee, Y.S. Park, K.B. Yoon, Angew. Chem. Int. Ed. 39 (2000) 950;
(d) A. Kulak, Y.S. Park, Y.-J. Lee, Y.S. Chun, K. Ha, K.B. Yoon, J. Am. Chem. Soc. 122 (2000) 9308;
(e) G.S. Lee, Y.-J. Lee, K. Ha, K.B. Yoon, Tetrahedron 56 (2000) 6965;
(f) Y.S. Chun, K. Ha, Y.-J. Lee, J.S. Lee, H.S. Kim, Y.S. Park, K.B. Yoon, Chem. Commun. (2002) 1846.
[4] (a) K. Ha, Y.-J. Lee, D.Y. Jung, J.H. Lee, K.B. Yoon, Adv. Mater. 12 (2000) 1614;
(b) K. Ha, Y.-L. Lee, Y.S. Chun, Y.S. Park, G.S. Lee, K.B. Yoon, Adv. Mater. 13 (2001) 594.
[5] G. Calzaferri, M. Pauchard, H. Maas, S. Huber, A. Khatyr, T. Schaafsma, J. Mater. Chem. 12 (2002) 1.
[6] G. Schulz-Ekloff, D. Wöhrle, B. van Duffel, R.A. Schoonheydt, Micropor. Mesopor. Mater. 51 (2002) 91.
[7] S. Hashimoto, J. Photochem. Photobiol. C: Photochem. Rev. 4 (2003) 19.
[8] S. Megelski, G. Calzaferri, Adv. Funct. Mater. 11 (2001) 277.
[9] (a) M. Kasha, H.R. Rawls, M. Ashraf El-Bayoumi, Pure Appl. Chem. 11 (1965) 371;
(b) E.G. McRae, M. Kasha, J. Chem. Phys. 28 (1958) 721.
[10] J.R. Lakowicz, Principles of Fluorescence Spectroscopy, Academic/Plenum, New York, 1999.
[11] M. Pauchard, A. Devaux, G. Calzaferri, Chem. Eur. J. 6 (2000) 3456.
[12] G. Calzaferri, D. Brühwiler, S. Megelski, M. Pfenniger, M. Pauchard, B. Hennessy, H. Maas, A. Devaux, U. Graf, Solid State Sci. 2 (2000) 421.
[13] (a) M.L. Cano, V. Fornés, H. García, M.A. Miranda, J. Pérez-Prieto, J. Chem. Soc., Chem. Commun. (1995) 2477;
(b) H. García, S. García, J. Pérez-Prieto, J.C. Scaiano, J. Phys. Chem. 100 (1996) 18158.
[14] D. Brühwiler, N. Gfeller, G. Calzaferri, J. Phys. Chem. B 102 (1998) 2923.
[15] N. Gfeller, S. Megelski, G. Calzaferri, J. Phys. Chem. B 102 (1998) 2433.
[16] M.M. Yatskou, M. Meyer, S. Huber, M. Pfenniger, G. Calzaferri, ChemPhysChem 4 (2003) 567.
[17] M. Pfenniger, G. Calzaferri, ChemPhysChem 1 (2000) 211.
[18] H. Maas, A. Khatyr, G. Calzaferri, Micropor. Mesopor. Mater. 65 (2003) 233.
[19] F. Laeri, O. Bossart, S. Huber, G. Calzaferri, Internal Report, March 2003.
[20] S. Hashimoto, M. Hagiri, N. Matsubara, S. Tobita, Phys. Chem. Chem. Phys. 3 (2001) 5043.
[21] X. Liu, J.K. Thomas, Chem. Mater. 6 (1994) 2303.
[22] (a) G. Calzaferri, N. Gfeller, J. Phys. Chem. 96 (1992) 3428;
(b) V. Ramamurthy, D.R. Sanderson, D.F. Eaton, J. Am. Chem. Soc. 115 (1993) 10438.
[23] M. Pauchard, Ph.D. Thesis, Department of Chemistry and Biochemistry, University of Bern, Switzerland, 2001.
[24] G. Calzaferri, S. Huber, H. Maas, C. Minkowski, Angew. Chem. Int. Ed. 42 (2003) 3732.
[25] (a) F. Binder, G. Calzaferri, N. Gfeller, Sol. Energy Mater. Sol. Cells 38 (1995) 175;
(b) F. Binder, G. Calzaferri, N. Gfeller, Proc. Indian Acad. Sci. (Chem. Sci.) 107 (1995) 753.
[26] (a) D.T. Theodorou, R.Q. Snurr, A.T. Bell, in: G. Alberti, T. Bein (Eds.), Comprehensive Supramolecular Chemistry, vol. 7, Elsevier, Oxford, 1996, p. 507;
(b) U. Schemmert, J. Kärger, J. Weitkamp, Micropor. Mesopor. Mater. 32 (1999) 101.
[27] S. Hashimoto, M. Hagiri, A.V. Barzykin, J. Phys. Chem. B 106 (2002) 844.
[28] H. Jobic, A.N. Fitch, J. Combet, J. Phys. Chem. B 104 (2000) 8491.
[29] D.E. Favre, D.J. Schaefer, S.M. Auerbach, B.F. Chmelka, Phys. Rev. Lett. 81 (1998) 5852.
[30] S. Hashimoto, T. Miyashita, M. Hagiri, J. Phys. Chem. B 103 (1999) 9149.
[31] (a) D. Brühwiler, R. Seifert, G. Calzaferri, J. Phys. Chem. B 103 (1999) 6397;
(b) D. Brühwiler, C. Leiggener, S. Glaus, G. Calzaferri, J. Phys. Chem. B 106 (2002) 3770.
[32] C. Leiggener, D. Brühwiler, G. Calzaferri, J. Mater. Chem. 13 (2003) 1969.
[33] G. Calzaferri, H. Maas, M. Pauchard, M. Pfenniger, S. Megelski, A. Devaux, in: D.C. Neckers, G. von Bünau, W.S. Jenks (Eds.), Advances in Photochemistry, vol. 27, John Wiley & Sons, 2002, p. 1.
[34] M. Pauchard, S. Huber, R. Méallet-Renault, H. Maas, R. Pansu, G. Calzaferri, Angew. Chem. Int. Ed. 40 (2001) 2839.
[35] B. Hennessy, S. Megelski, C. Marcolli, V. Shklover, C. Bärlocher, G. Calzaferri, J. Phys. Chem. B 103 (1999) 3340.
[36] (a) B.R. Müller, G. Calzaferri, J. Chem. Soc., Faraday Trans. 92 (1996) 1633;
(b) B.R. Müller, G. Calzaferri, Micropor. Mesopor. Mater. 21 (1998) 59.
[37] S. Megelski, A. Lieb, M. Pauchard, A. Drechsler, S. Glaus, C. Debus, A.J. Meixner, G. Calzaferri, J. Phys. Chem. B 105 (2001) 25.
[38] (a) K. Hoffmann, F. Marlow, J. Caro, Adv. Mater. 9 (1997) 567;
(b) K. Hoffmann, U. Resch-Genger, F. Marlow, Micropor. Mesopor. Mater. 41 (2000) 99;
(c) K. Hoffmann, U. Resch-Genger, F. Marlow, in: F. Laeri, F. Schüth, U. Simon, M. Wark (Eds.), Host-Guest Systems Based on Nanoporous Crystals, Wiley–VCH, 2003, p. 501.
[39] (a) H.L. Casal, J.C. Scaiano, Can. J. Chem. 62 (1984) 628;
(b) H.L. Casal, J.C. Scaiano, Can. J. Chem. 63 (1985) 1308;
(c) J.C. Scaiano, H. García, Acc. Chem. Res. 32 (1999) 783.
[40] (a) T. Förster, Ann. Phys. (Leipzig) 2 (1948) 55;
(b) T. Förster, Fluoreszenz organischer Verbindungen, Vandenhoeck & Ruprecht, Göttingen, 1951.
[41] N. Gfeller, G. Calzaferri, J. Phys. Chem. B 101 (1997) 1396.
[42] N. Gfeller, S. Megelski, G. Calzaferri, J. Phys. Chem. B 103 (1999) 1250.
[43] (a) V. Ramamurthy, J.V. Casper, D.F. Eaton, E.W. Kuo, D.R. Corbin, J. Am. Chem. Soc. 114 (1992) 3882;
(b) V. Ramamurthy, J.V. Casper, D.R. Corbin, D.F. Eaton, J. Photochem. Photobiol. A: Chem. 50 (1989) 157.
[44] S.J. Hawkes, J. Chem. Educ. 73 (1996) 516.
[45] (a) B.G. Silbernagel, A.R. Garcia, J.M. Newsam, R. Hulme, J. Phys. Chem. 93 (1989) 6506;
(b) J.M. Newsam, J. Phys. Chem. 93 (1989) 7689;
(c) J.C. Ma, D.A. Dougherty, Chem. Rev. 97 (1997) 1303.
[46] L.S. Kaanumalle, J. Sivaguru, R.B. Sunoj, P.H. Lakshminarasimhan, J. Chandrasekhar, V. Ramamurthy, J. Org. Chem. 67 (2002) 8711.
[47] C. Kirschhock, H. Fuess, Zeolites 17 (1996) 381.
[48] H. Maas, G. Calzaferri, Angew. Chem. Int. Ed. 41 (2002) 2284.
[49] A. Khatyr, H. Maas, G. Calzaferri, J. Org. Chem. 67 (2002) 6705.

[50] (a) N.R.E.N. Impens, P. van der Voort, E.F. Vansant, Micropor. Mesopor. Mater. 28 (1999) 217;
(b) K.M.R. Kallury, P.M. Macdonald, M. Thompson, Langmuir 10 (1994) 492.
[51] A.S.T. Chiang, K. Chao, J. Phys. Chem. Solids 62 (2001) 1899.
[52] J.S. Lee, Y.-J. Lee, E.L. Tae, Y.S. Park, K.B. Yoon, Science 301 (2003) 818.
[53] (a) J. Caro, G. Finger, J. Kornatowski, J. Richter-Mendau, L. Werner, B. Zibrowius, Adv. Mater. 4 (1992) 273;
(b) J. Caro, G. Finger, E. Jahn, J. Kornatowski, F. Marlow, M. Noack, L. Werner, B. Zibrowius, in: R. von Ballmoos, D.B. Higgins, M.M.J. Treacy (Eds.), Proceedings of the 9th International Zeolite Conference, Butterworth–Heinemann, Stoneham, MA, 1993, p. 683.
[54] L. Scandella, G. Binder, J. Gobrecht, J.C. Jansen, Adv. Mater. 8 (1996) 137.
[55] J. Caro, F. Marlow, M. Wübbenhorst, Adv. Mater. 6 (1994) 413.
[56] (a) H. Maas, G. Calzaferri, Spectrum 16 (2003) 18;
(b) S. Huber, G. Calzaferri, ChemPhysChem 2 (2004) 239.
[57] D.L. Dexter, J. Lumin. 18/19 (1979) 779.
[58] Nanoscale Materials, Acc. Chem. Res. 32 (1999) 387 (special issue).
[59] G.A. Ozin, Adv. Mater. 4 (1992) 612.
[60] (a) C.R. Berry, Phys. Rev. 161 (1967) 848;
(b) L. Brus, J. Phys. Chem. 90 (1986) 2555;
(c) A.P. Alivisatos, Science 271 (1996) 933;
(d) A.P. Alivisatos, J. Phys. Chem. 100 (1996) 13226.
[61] T. Vossmeyer, L. Katsikas, M. Giersig, I.G. Popovic, K. Diesner, A. Chemseddine, A. Eychmüller, H. Weller, J. Phys. Chem. 98 (1994) 7665.
[62] J. Nanda, S. Sapra, D.D. Sarma, N. Chandrasekharan, G. Hodes, Chem. Mater. 12 (2000) 1018.
[63] F.W. Wise, Acc. Chem. Res. 33 (2000) 773.
[64] N. Herron, Y. Wang, M.M. Eddy, G.D. Stucky, D.E. Cox, K. Moller, T. Bein, J. Am. Chem. Soc. 111 (1989) 530.
[65] Y. Wang, N. Herron, J. Phys. Chem. 91 (1987) 257.
[66] A. Jentys, R.W. Grimes, J.D. Gale, C.R.A. Catlow, J. Phys. Chem. 97 (1993) 13535.
[67] X. Liu, J.K. Thomas, Langmuir 5 (1989) 58.
[68] H. Peng, S.M. Liu, L. Ma, Z.J. Lin, S.J. Wang, J. Cryst. Growth 224 (2001) 274.
[69] (a) M. Wark, G. Schulz-Ekloff, N.I. Jaeger, Catal. Today 8 (1991) 467;
(b) M. Wark, G. Schulz-Ekloff, N.I. Jaeger, A. Zukal, Stud. Surf. Sci. Catal. 69 (1991) 189;
(c) M. Wark, G. Schulz-Ekloff, N.I. Jaeger, W. Lutz, Mater. Res. Soc. Symp. Proc. 233 (1991) 133.
[70] R.J. Myers, J. Chem. Educ. 63 (1986) 687.
[71] K. Moller, T. Bein, N. Herron, W. Mahler, Y. Wang, Inorg. Chem. 28 (1989) 2914.
[72] F. Iacomi, A. Vasile, E.K. Polychroniadis, Mater. Sci. Eng. B 101 (2003) 275.
[73] F. Márquez, V. Fornés, Solid State Commun. 112 (1999) 17.
[74] C.L. Bowes, G.A. Ozin, J. Mater. Chem. 8 (1998) 1281.
[75] Y. Okamoto, H. Okamoto, T. Kubota, H. Kobayashi, O. Terasaki, J. Phys. Chem. B 103 (1999) 7160.
[76] L. Motte, M.P. Pileni, J. Phys. Chem. B 102 (1998) 4104.
[77] K. Akamatsu, S. Takei, M. Mizuhata, A. Kajinami, S. Deki, S. Takeoka, M. Fujii, S. Hayashi, K. Yamamoto, Thin Solid Films 359 (2000) 55.
[78] H.W. Rollins, F. Lin, J. Johnson, J.J. Ma, J.T. Liu, M.H. Tu, D.D. DesMarteau, Y.P. Sun, Langmuir 16 (2000) 8031.
[79] L. Armelao, R. Bertoncello, E. Cattaruzza, S. Gialanella, S. Gross, G. Mattei, P. Mazzoldi, E. Tondello, J. Mater. Chem. 12 (2002) 2401.
[80] S.H. Liu, X.F. Qian, J. Yin, L. Hong, X.L. Wang, Z.K. Zhu, J. Solid State Chem. 168 (2002) 259.
[81] (a) M.C. Brelle, J.Z. Zhang, L. Nguyen, R.K. Mehra, J. Phys. Chem. A 103 (1999) 10194;
(b) Y.P. Sun, J.E. Riggs, H.W. Rollins, R. Guduru, J. Phys. Chem. B 103 (1999) 77.
[82] T.G. Schaaff, A.J. Rodinone, J. Phys. Chem. B 107 (2003) 10416.
[83] (a) T. Tani, J. Imaging Sci. Technol. 39 (1995) 386;
(b) J.W. Mitchell, J. Imaging Sci. Technol. 42 (1998) 215;
(c) E. Charlier, M. Van Doorselaer, R. Gijbels, R. De Keyzer, I. Geuens, J. Imaging Sci. Technol. 44 (2000) 235;
(d) R.C. Baetzold, J. Imaging Sci. Technol. 43 (1999) 375.
[84] M. Rálek, P. Jíru, O. Grubner, H. Beyer, Collect. Czech. Chem. Commun. 27 (1962) 142.
[85] T. Sun, K. Seff, Chem. Rev. 94 (1994) 857.
[86] R. Seifert, A. Kunzmann, G. Calzaferri, Angew. Chem. Int. Ed. 37 (1998) 1522.
[87] (a) R. Beer, G. Calzaferri, I. Kamber, J. Chem. Soc., Chem. Commun. (1991) 1489;
(b) G. Calzaferri, R. Giovanoli, I. Kamber, V. Shklover, R. Nesper, Res. Chem. Intermed. 19 (1993) 31.
[88] G. Calzaferri, C. Leiggener, S. Glaus, D. Schürch, K. Kuge, Chem. Soc. Rev. 32 (2003) 29.
[89] R. Seifert, R. Rytz, G. Calzaferri, J. Phys. Chem. A 104 (2000) 7473.
[90] A. Kunzmann, R. Seifert, G. Calzaferri, J. Phys. Chem. B 103 (1999) 18.
[91] A.A. Bagatur'yants, A.A. Safonov, H. Stoll, H.-J. Werner, J. Chem. Phys. 109 (1998) 3096.
[92] R. Sadanaga, S. Sueno, Mineral. J. 5 (1967) 124.
[93] P. Junod, H. Hediger, B. Kilchör, J. Wullschleger, Philos. Mag. 36 (1977) 941.
[94] W. DeWilde, G. Peeters, J.H. Lunsford, J. Phys. Chem. 84 (1980) 2306.
[95] P. Lainé, M. Lanz, G. Calzaferri, Inorg. Chem. 35 (1996) 3514.
[96] D.W. Breck, Zeolite Molecular Sieves, John Wiley, New York, 1974.
[97] (a) C.T. Kresge, M.E. Leonowicz, W.J. Roth, J.C. Vartuli, J.S. Beck, Nature 359 (1992) 710;
(b) J.S. Beck, J.C. Vartuli, W.J. Roth, M.E. Leonowicz, C.T. Kresge, K.D. Schmitt, C.T.-W. Chu, D.H. Olson, E.W. Sheppard, S.B. McCullen, J.B. Higgins, J.L. Schlenker, J. Am. Chem. Soc. 114 (1992) 10834.
[98] K. Moller, T. Bein, Chem. Mater. 10 (1998) 2950.
[99] J.M. Gómez, J. Deere, D. Goradia, J. Cooney, E. Magner, B.K. Hodnett, Catal. Lett. 88 (2003) 183, and references therein.
[100] X.S. Zhao, G.Q. Lu, A.K. Whittaker, G.J. Millar, H.Y. Zhu, J. Phys. Chem. B 101 (1997) 6525.
[101] H. Landmesser, H. Kosslick, W. Storek, R. Fricke, Solid State Ionics 101–103 (1997) 271.
[102] C. Pophal, H. Fuess, Micropor. Mesopor. Mater. 33 (1999) 241.
[103] J.Y. Kim, S.H. Park, J.-S. Yu, Opt. Mater. 21 (2002) 349.
[104] (a) D.S. Shephard, W. Zhou, T. Maschmeyer, J.M. Matters, C.L. Roper, S. Parsons, B.F.G. Johnson, M.J. Duer, Angew. Chem. Int. Ed. 37 (1998) 2719;
(b) Y. Rohlfing, D. Wöhrle, M. Wark, G. Schulz-Ekloff, J. Rathousky, A. Zukal, Stud. Surf. Sci. Catal. 129 (2000) 295.
[105] (a) Y. Rohlfing, D. Wöhrle, J. Rathousky, A. Zukal, M. Wark, Stud. Surf. Sci. Catal. 142 (2002) 1067;
(b) M. Wark, M. Ganschow, Y. Rohlfing, G. Schulz-Ekloff, D. Wöhrle, Stud. Surf. Sci. Catal. 135 (2001) 3292.
[106] M. Ganschow, M. Wark, D. Wöhrle, G. Schulz-Ekloff, Angew. Chem. Int. Ed. 39 (2000) 161.

[107] M. Wark, Y. Rohlfing, Y. Altindag, H. Wellmann, Phys. Chem. Chem. Phys. 5 (2003) 5188.
[108] C.E. Fowler, B. Lebeau, S. Mann, Chem. Commun. (1998) 1825.
[109] I. Kinski, H. Gies, F. Marlow, Zeolites 19 (1997) 375.
[110] (a) N.K. Mal, M. Fujiwara, Y. Tanaka, Nature 421 (2003) 350; (b) N.K. Mal, M. Fujiwara, Y. Tanaka, T. Taguchi, M. Matsukata, Chem. Mater. 15 (2003) 3385.
[111] C.-Y. Lai, B.G. Trewyn, D.M. Jeftinija, K. Jeftinija, S. Xu, S. Jeftinija, V.S.-Y. Lin, J. Am. Chem. Soc. 125 (2003) 4451.
[112] A. Stein, B.J. Melde, R.C. Schroden, Adv. Mater. 12 (2000) 1403.
[113] D. Brunel, N. Bellocq, P. Sutra, A. Cauvel, M. Laspéras, P. Moreau, F. Di Renzo, A. Galarneau, F. Fajula, Coord. Chem. Rev. 178–180 (1998) 1085.
[114] R. Anwander, Chem. Mater. 13 (2001) 4419.
[115] D.E. De Vos, M. Dams, B.F. Sels, P.A. Jacobs, Chem. Rev. 102 (2002) 3615.
[116] A. Corma, Chem. Rev. 97 (1997) 2373.
[117] (a) M. Anpo, H. Yamashita, K. Ikeue, Y. Fujii, S.G. Zhang, Y. Ichihashi, D.R. Park, Y. Suzuki, K. Koyano, T. Tatsumi, Catal. Today 44 (1998) 327; (b) H. Yamashita, Y. Fujii, Y. Ichihashi, S.G. Zhang, K. Ikeue, D.R. Park, K. Koyano, T. Tatsumi, M. Anpo, Catal. Today 45 (1998) 221; (c) M. Anpo, S. Higashimoto, Y. Shioya, K. Ikeue, M. Harada, M. Watanabe, Stud. Surf. Sci. Catal. 140 (2001) 27; (d) M. Anpo, M. Takeuchi, J. Catal. 216 (2003) 505.
[118] (a) R. Tsumura, S. Higashimoto, M. Matsuoka, H. Yamashita, M. Che, M. Anpo, Catal. Lett. 68 (2000) 101; (b) S. Higashimoto, R. Tsumura, M. Matsuoka, H. Yamashita, M. Che, M. Anpo, Stud. Surf. Sci. Catal. 140 (2001) 315.
[119] (a) A. Corma, M.T. Navarro, J. Pérez-Pariente, J. Chem. Soc., Chem. Commun. (1994) 147; (b) W. Zhang, M. Fröba, J. Wang, P.T. Tanev, J. Wong, T.J. Pinnavaia, J. Am. Chem. Soc. 118 (1996) 9164; (c) M. Morey, A. Davidson, G. Stucky, Micropor. Mater. 6 (1996) 99; (d) F. Rey, G. Sankar, T. Maschmeyer, J.M. Thomas, R.G. Bell, G.N. Greaves, Top. Catal. 3 (1996) 121; (e) A.M. Prakash, H.M. Sung-Suh, L. Kevan, J. Phys. Chem. B 102 (1998) 857.
[120] (a) K. Chaudhari, R. Bal, T.K. Das, A. Chandwadkar, D. Srinivas, S. Sivasanker, J. Phys. Chem. B 104 (2000) 11066; (b) X.X. Wang, F. Lefebvre, J. Patarin, J.-M. Basset, Micropor. Mesopor. Mater. 42 (2001) 269.
[121] S. Lim, G.L. Haller, J. Phys. Chem. B 106 (2002) 8437, and references therein.
[122] M. Ziolek, I. Nowak, B. Kilos, I. Sobczak, P. Decyk, M. Trejda, J.C. Volta, J. Phys. Chem. Solids 65 (2004) 571, and references therein.
[123] W.A. Carvalho, P.B. Varaldo, M. Wallau, U. Schuchardt, Zeolites 18 (1997) 408.
[124] N. Lang, P. Delichere, A. Tuel, Micropor. Mesopor. Mater. 56 (2002) 203, and references therein.
[125] T. Maschmeyer, Curr. Opin. Solid State Mater. Sci. 3 (1998) 71.
[126] T. Maschmeyer, F. Rey, G. Sankar, J.M. Thomas, Nature 378 (1995) 159.
[127] R.D. Oldroyd, J.M. Thomas, T. Maschmeyer, P.A. MacFaul, D.W. Snelgrove, K.U. Ingold, D.D.M. Wayner, Angew. Chem. Int. Ed. 35 (1996) 2787.
[128] (a) M.S. Morey, G.D. Stucky, S. Schwarz, M. Fröba, J. Phys. Chem. B 103 (1999) 2037; (b) W.H. Zhang, J.L. Shi, L.Z. Wang, D.S. Yan, Mater. Lett. 46 (2000) 35; (c) X.-X. Wang, L. Veyre, F. Lefebvre, J. Patarin, J.-M. Basset, Micropor. Mesopor. Mater. 66 (2003) 169.
[129] (a) Z. Luan, L. Kevan, J. Phys. Chem. B 101 (1997) 2020; (b) K. Zhu, Z. Ma, Y. Zou, W. Zhou, T. Chen, H. He, Chem. Commun. (2001) 2552; (c) M. Morey, A. Davidson, H. Eckert, G. Stucky, Chem. Mater. 8 (1996) 486; (d) P. Van Der Voort, M. Morey, G.D. Stucky, M. Mathieu, E.F. Vansant, J. Phys. Chem. B 102 (1998) 585; (e) R.D. Oldroyd, G. Sankar, J.M. Thomas, M. Hunnius, W.F. Maier, J. Chem. Soc., Faraday Trans. 94 (1998) 3177.
[130] R.R. Rao, B.M. Weckhuysen, R.A. Schoonheydt, Chem. Commun. (1999) 445.
[131] I.J. Shannon, T. Maschmeyer, R.D. Oldroyd, G. Sankar, J.M. Thomas, H. Perrot, J.P. Balikdjian, M. Che, J. Chem. Soc., Faraday Trans. 94 (1998) 1495.
[132] M.S. Morey, J.D. Bryan, S. Schwarz, G.D. Stucky, Chem. Mater. 12 (2000) 3435.
[133] (a) C. Nozaki, C.G. Lugmair, A.T. Bell, T.D. Tilley, J. Am. Chem. Soc. 124 (2002) 13194; (b) M. Stockenhuber, M.J. Hudson, R.W. Joyner, J. Phys. Chem. B 104 (2000) 3370.
[134] D. Brühwiler, H. Frei, J. Phys. Chem. B 107 (2003) 8547.
[135] M. Pillinger, C.D. Nunes, P.D. Vaz, A.A. Valente, I.S. Gonçalves, P.J.A. Ribeiro-Claro, J. Rocha, L.D. Carlos, F.E. Kühn, Phys. Chem. Chem. Phys. 4 (2002) 3098.
[136] R. Anwander, H.W. Görlitzer, G. Gerstberger, C. Palm, O. Runte, M. Spiegler, J. Chem. Soc., Dalton Trans. (1999) 3611.
[137] (a) L. Bonneviot, O. Legendre, M. Kermarec, D. Olivier, M. Che, J. Colloid Interf. Sci. 134 (1990) 534; (b) J.-F. Lambert, M. Hoogland, M. Che, J. Phys. Chem. B 101 (1997) 10347.
[138] J.-M. Basset, F. Lefebvre, C. Santini, Coord. Chem. Rev. 178–180 (1998) 1703.
[139] (a) O. Clause, M. Kermarec, L. Bonneviot, F. Villain, M. Che, J. Am. Chem. Soc. 114 (1992) 4709; (b) J.Y. Carriat, M. Che, M. Kermarec, M. Verdaguer, A. Michalowicz, J. Am. Chem. Soc. 120 (1998) 2059.
[140] J.F. Díaz, K.J. Balkus, F. Bedioui, V. Kurshev, L. Kevan, Chem. Mater. 9 (1997) 61.
[141] S. Boujday, J.-F. Lambert, M. Che, J. Phys. Chem. B 107 (2003) 651.
[142] Z. Luan, P.A. Meloni, R.S. Czernuszewicz, L. Kevan, J. Phys. Chem. B 101 (1997) 9046.
[143] (a) Y.H. Yeom, H. Frei, J. Phys. Chem. A 106 (2002) 3350; (b) Y.H. Yeom, H. Frei, J. Phys. Chem. A 105 (2001) 5334; (c) N. Ulagappan, H. Frei, J. Phys. Chem. A 104 (2000) 7834; (d) N. Ulagappan, H. Frei, J. Phys. Chem. A 104 (2000) 490.
[144] P. Behrens, G.D. Stucky, in: G. Alberti, T. Bein (Eds.), Comprehensive Supramolecular Chemistry, vol. 7, Elsevier, Oxford, 1996, p. 721.
[145] C. Baerlocher, W.M. Meier, D.H. Olson, Atlas of Zeolite Framework Types, Elsevier, Amsterdam, 2001.
[146] (a) U. Ciesla, F. Schüth, Mircopor. Mesopor. Mater. 27 (1999) 131; (b) J.Y. Ying, C.P. Mehnert, M.S. Wong, Angew. Chem. Int. Ed. 38 (1999) 56; (c) G. Øye, J. Sjöblom, M. Stöcker, Adv. Colloid Interf. Sci. 89–90 (2001) 439.
[147] R.A. Schoonheydt, in: G. Alberti, T. Bein (Eds.), Comprehensive Supramolecular Chemistry, vol. 7, Elsevier, Oxford, 1996, p. 337.
[148] (a) J. Gierschner, H.-J. Egelhaaf, H.-G. Mack, D. Oelkrug, R. Martinez-Alvarez, M. Hanack, Synth. Met. 137 (2003) 1449; (b) C. Botta, S. Destri, M. Pasini, P. Picouet, G. Bongiovanni, A. Mura, M. Uslenghi, G. Di Silvestro, R. Tubino, Synth. Met. 139 (2003) 791.